

Probing the chiral and $U(1)$ axial symmetry restoration via meson susceptibilities in holographic QCD

Hiwa A. Ahmed,^{1,*} Danning Li,^{2,†} Mamiya Kawaguchi,^{3,‡} and Mei Huang^{4,§}

¹*Charmo Center for Research, Training and Consultancy,
Charmo University, 46023, Chamchamal, Sulaymaniyah, Iraq*

²*Department of Physics and Siyuan Laboratory, Jinan University, Guangzhou 510632, P.R. China*

³*Center for Fundamental Physics, School of Mechanics and Photoelectric Physics,*

Anhui University of Science and Technology, Huainan, Anhui 232001, People's Republic of China

⁴*School of Nuclear Science and Technology, University of Chinese Academy of Sciences, Beijing 100049, China*

(Dated: March 16, 2026)

We investigate the restoration patterns of chiral and $U(1)$ axial symmetries at finite temperature using a soft-wall holographic QCD model. The study employs two distinct parameter sets (Case I and Case II), both calibrated to reproduce a pseudocritical temperature $T_{pc} \sim 155$ MeV and the physical pion mass. The temperature dependence of the light and strange quark condensates confirms a smooth chiral crossover transition, with pseudocritical temperatures of $T_{pc} = 0.157$ GeV and $T_{pc} = 0.154$ GeV for Cases I and II, respectively. The screening masses of chiral partner mesons (π - σ and η - a_0) become degenerate near T_{pc} , providing a clear signature of chiral symmetry restoration. Analysis of the corresponding meson susceptibilities further supports this conclusion. However, the indicator for $U(1)$ axial symmetry restoration, $\chi_\pi - \chi_{a_0}$, vanishes at a temperature $T \sim 0.190$ GeV, which indicates a distinct restoration scale with chiral symmetry restoration scale within the present holographic framework. The temperature-dependent topological susceptibility $\chi_{top}^{1/4}$ is also computed, showing a sharp drop near T_{pc} and a subsequent slight decrease. While the model qualitatively captures established features of the chiral transition, the results highlight a limitation in the qualitative description of the $U(1)$ axial anomaly compared to LQCD in our work.

I. INTRODUCTION

In the study of quantum chromodynamics (QCD), there is significant interest in understanding the restoration of chiral symmetry and the $U(1)$ axial ($U(1)_A$) anomaly under extreme conditions such as high temperature or density. In the massless quark limit (chiral limit), the QCD Lagrangian exhibits chiral symmetry; however, this symmetry is spontaneously broken in the vacuum, giving rise to the hadron mass spectrum and other key properties [1]. The $U(1)_A$ symmetry, explicitly broken by the quantum anomaly, is equally vital for understanding non-perturbative QCD phenomena, such as the large mass of the η' meson [2]. The restoration of these symmetries during the transition from hadronic matter to the quark-gluon plasma (QGP) provides critical insights into the phase structure of QCD and the properties of matter in the early universe.

A powerful framework for probing these symmetry restorations is provided by meson and topological susceptibilities. The symmetry breakings in QCD are directly reflected in meson susceptibility functions, which are defined as the two-point functions of quark bilinear operators in the low-energy limit [3–13]. At high temperatures, as chiral symmetry is restored, the masses and susceptibilities of mesons related by chiral transformations become degenerate. This degeneracy allows meson susceptibilities to serve as a quantitative measure of chiral symmetry breaking and its restoration. Similarly, the effective restoration of the $U(1)_A$ symmetry can be quantified by the degeneracies between meson susceptibility functions connected by the $U(1)_A$ transformation.

The role of the $U(1)_A$ anomaly can be further quantified through the topological susceptibility, which is sensitive to fluctuations of the topological charge in the QCD vacuum. By making use of the Ward-Takahashi identity (WTI) associated with chiral symmetry, one can show that the topological susceptibility is correlated with the chiral and $U(1)_A$ partner structures in the meson susceptibility functions [10–12, 14–16]. This establishes the topological susceptibility as a key indicator for the breaking strength of the $U(1)_A$ symmetry through the chiral phase transition. Lattice QCD simulations at physical quark masses confirm that the magnitude of the topological susceptibility smoothly decreases at high temperatures [17–19], providing direct evidence of the persistence anomaly and its subsequent suppression.

The restoration of chiral symmetry and the $U(1)_A$ symmetry are suggested to be connected, although the precise nature of this connection, especially its dependence on the number of quark flavors, is still not fully understood. A

* hiwa.ahmed@chu.edu.iq

† lidanning@jnu.edu.cn

‡ mamiya@aust.edu.cn

§ huangmei@ucas.ac.cn

strong correlation between the topological susceptibility and chiral restoration has been extensively studied through meson susceptibility functions, both within 2-flavor QCD [3, 4, 20, 21] and 2 + 1-flavor QCD [5, 6, 22]. Furthermore, the $U(1)_A$ anomaly contribution remains manifest in meson susceptibility functions at high temperatures even when the light quarks are tuned to be massless, highlighting its fundamental and non-trivial impact on the phase structure of QCD [23].

Calculating the low-energy two-point correlation functions requires a non-perturbative technique that lies beyond the reach of conventional perturbative QCD. One powerful non-perturbative approach is the Anti-de Sitter/Conformal Field Theory (AdS/CFT) correspondence, or gauge/gravity duality [24, 25]. Holographic QCD models built on this duality are broadly categorized into two approaches. The top-down approach starts from a consistent string theory in higher dimensions and derives a lower-dimensional theory with QCD-like properties [26, 27]. In contrast, the bottom-up approach begins with established QCD phenomenology and constructs a higher-dimensional gravitational dual that reproduces these features [28–34]. A significant development in the bottom-up approach is the soft-wall AdS/QCD model [30], where a specific dilaton configuration is introduced, which successfully generates the linear Regge trajectory of meson spectra and describes the spontaneous breaking of chiral symmetry in the chiral limit. In the soft-wall model, the phase structure has been studied at finite temperature and/or finite chemical potentials for different flavor systems [35–44]. Moreover, the thermal properties and dynamics of light-flavor mesons have been investigated via the two-point correlation function, with particular emphasis on the pseudo-Goldstone bosons emerging from the chiral phase transition [45, 46]. In this paper, we employ a holographic framework to calculate meson and topological susceptibilities, intending to investigate the restoration patterns of chiral and $U(1)_A$ symmetries at finite temperatures. Our work aims to provide a qualitative understanding of these critical QCD phenomena from a gravitational dual perspective.

The paper is organized as follows. Firstly, we will provide a brief introduction to the soft-wall AdS/QCD models for a three-flavor system and present the equations of motion in Section II. Then, in section III, we will derive the meson susceptibilities from the two-point correlation functions for scalar and pseudoscalar sectors. Additionally, we will obtain the topological susceptibilities in section IV. Referring to the results in section V, we will show the results of the order parameter (chiral condensate), screening mass, mesons, and topological susceptibilities. Finally, we will conclude the results in section VI.

II. SOFT-WALL MODEL AT FINITE TEMPERATURE

We begin with a brief review of the soft-wall holographic model. The model is defined in a five-dimensional Anti-de Sitter (AdS_5) spacetime [30]. Temperature is incorporated via a black hole geometry, described by a static background metric. Specifically, we adopt the AdS-Schwarzschild (AdS-SW) black hole solution [38, 39]:

$$ds^2 = e^{2A_s(z)} \left(f(z) dt^2 - \frac{1}{f(z)} dz^2 - dx_i dx^i \right), \quad (1)$$

where z is the holographic (fifth) coordinate. The scale function is given by $A_s(z) = -\log(z/L)$, scaled by the AdS curvature radius L (set to $L = 1$ for simplicity). The blackening factor is:

$$f(z) = 1 - \frac{z^4}{z_h^4}, \quad (2)$$

with z_h denoting the horizon location, defined by $f(z_h) = 0$. The Hawking temperature, identified as the temperature of the dual QCD system, is given by:

$$T = \frac{1}{4\pi} \left| \frac{df(z)}{dz} \right|_{z=z_h} = \frac{1}{\pi z_h}. \quad (3)$$

A. The 5D Holographic Action

Following the bottom-up approach to holographic QCD, we employ a five-dimensional gauge theory with $U(N_f)_L \times U(N_f)_R$ symmetry, where N_f is the number of quark flavors [28–30]. The model includes bulk left- (L_M) and right- (R_M) handed gauge fields. To incorporate the chiral condensation operator, a bulk scalar field X is introduced; it transforms in the bifundamental representation under the chiral symmetry. To break the conformal invariance, a dilaton background field $\Phi(z)$ is included, acting as a soft infrared (IR) cutoff [30].

The five-dimensional action for the soft-wall model is:

$$S_M = \int d^5x \sqrt{g} e^{-\Phi} \left\{ \text{Tr} \left[(D^M X)^\dagger (D_M X) - V(X) - \frac{1}{4g_5^2} (L^{MN} L_{MN} + R^{MN} R_{MN}) \right] - \gamma \text{Re}(\det[X]) \right\}, \quad (4)$$

where $g \equiv \det(g_{MN}) = e^{5A_s(z)} = z^{-5}$ is the determinant of the metric, and D^M is the covariant derivative which is $D^M X = \partial^M X - iL^M X + iXR^M$. The field strength tensors are $L_{MN} = \partial_M L_N - \partial_N L_M - i[L_M, L_N]$ and $R_{MN} = \partial_M R_N - \partial_N R_M - i[R_M, R_N]$. The gauge coupling g_5 is fixed by matching the vector current correlator to its QCD asymptotic form: $g_5^2 = 12\pi^2/N_c$. The parameter γ controls the strength of the determinant term, $\text{Re}(\det[X])$, which is anomalous under $U(1)_A$ but invariant under $SU(N_f)_L \times SU(N_f)_R$.

The scalar potential $V(X)$ is taken to be:

$$V(X) = m_5^2 \text{Tr}(X^\dagger X) + \lambda \text{Tr}(|X|^4), \quad (5)$$

where the five-dimensional mass parameter, from the AdS/CFT dictionary, is $m_5^2 = (\Delta - p)(\Delta + p - 4) = -3$ for $\Delta = 3$ and $p = 0$. The positive dimensionless coupling λ is introduced to ensure a non-vanishing quark condensate in the chiral limit ($m_q \rightarrow 0$); without this term, the condensate would accidentally vanish [47].

In the soft-wall model, there are different ways to get a consistent meson spectrum with the experimental data and a good description of the chiral phase transition. Here we consider the following two cases:

1. Case I: The specific profile of the dilaton field, which respects both the IR and UV behavior with a standard 5D mass [38, 39],

$$\Phi(z) = -\mu_1^2 z^2 + (\mu_1^2 + \mu_g^2) z^2 \tanh(\mu_2^2 z^2) \quad \& \quad m_5^2 = -3. \quad (6)$$

2. Case II: An IR-modified soft-wall AdS/QCD model with a modified 5D mass and quadratic dilaton field [41]¹,

$$\Phi(z) = \mu_g^2 z^2 \quad \& \quad m_5^2 = -3 - \mu_c^2 z^2. \quad (7)$$

We analyze both variants of the model (Case I and Case II). To study chiral symmetry breaking, we consider the static, homogeneous expectation value of the scalar field X , which takes the form:

$$X(z) = X_0(z) = \text{diag} \left(\frac{\chi_l(z)}{2}, \frac{\chi_l(z)}{2}, \frac{\chi_s(z)}{2} \right), \quad (8)$$

where we impose isospin symmetry ($m_u = m_d \equiv m_l$). This implies the light quark components are equal: $\chi_u(z) = \chi_d(z) \equiv \chi_l(z)$, while $\chi_s(z)$ corresponds to the strange quark sector.

To isolate the dynamics of the chiral condensate, we set the bulk gauge fields to zero ($L_M = R_M = 0$). With this simplification, the full action (4) reduces to an effective action for the scalar VEVs, χ_l and χ_s :

$$S[\chi_l, \chi_s] = \int d^5x \sqrt{g} e^{-\Phi} \left\{ g^{zz} \left(\frac{1}{2} \chi_l'^2 + \frac{1}{4} \chi_s'^2 \right) - \left(\frac{1}{2} m_5^2 \chi_l^2 + \frac{1}{4} m_5^2 \chi_s^2 + \frac{\lambda}{8} \chi_l^4 + \frac{\lambda}{16} \chi_s^4 + \frac{\gamma}{8} \chi_l^2 \chi_s \right) \right\} \quad (9)$$

where $g^{zz} = -e^{-2A_s(z)} f(z)$ is the relevant component of the inverse metric.

B. Equations of Motion

Varying the effective action (9) yields the following equations of motion (EOMs) for the fields $\chi_f(z)$ ($f = l, s$):

$$\begin{aligned} \chi_l'' + \left(3A_s' - \Phi' + \frac{f'}{f} \right) \chi_l' - \frac{e^{2A_s}}{f} \left(m_5^2 + \frac{\gamma}{4} \chi_s + \frac{\lambda}{2} \chi_l^2 \right) \chi_l &= 0, \\ \chi_s'' + \left(3A_s' - \Phi' + \frac{f'}{f} \right) \chi_s' - \frac{e^{2A_s}}{f} \left(m_5^2 \chi_s + \frac{\gamma}{4} \chi_l^2 + \frac{\lambda}{2} \chi_s^3 \right) &= 0, \end{aligned} \quad (10)$$

¹ While other modifications that likewise introduce an additional scale to characterize chiral dynamics are conceivable (see, e.g., Refs. [48, 49]), the present discussion is restricted to the two classes outlined above.

where the prime (') denotes a derivative with respect to the holographic coordinate z .

The asymptotic behavior of the fields $\chi_l(z)$ and $\chi_s(z)$ in the ultraviolet (UV, $z \rightarrow 0$) and infrared (IR, $z \rightarrow z_h$) regions is derived for the two model variants, characterized by their distinct dilaton profiles $\Phi(z)$ and five-dimensional mass terms m_5^2 . The expansions are as follows:

Case I:

$$\begin{aligned}\chi_l(z \rightarrow 0) &= m_l \zeta z - \frac{\gamma}{4} m_l m_s \zeta^2 z^2 + \frac{m_l \zeta}{4} \left(-4\mu_1^2 + m_l^2 \zeta^2 \lambda - \frac{\gamma^2}{8} (m_l^2 \zeta^2 + m_s^2 \zeta^2) \right) z^3 \log(z) + \frac{\sigma_l}{\zeta} z^3, \\ \chi_l(z \rightarrow z_h) &= c_{l,0} - \frac{c_{l,0}(-2c_{l,0}^2 \lambda + 12 - \gamma c_{s,0})}{16z_h} (z_h - z) + \mathcal{O}[(z_h - z)^2],\end{aligned}\tag{11}$$

$$\begin{aligned}\chi_s(z \rightarrow 0) &= m_s \zeta z - \frac{\gamma}{4} m_l^2 \zeta^2 z^2 + \frac{1}{4} \left(-4\mu_1^2 m_s \zeta + m_s^3 \zeta^3 \lambda - \frac{\gamma^2}{4} m_l^2 m_s \zeta^3 \right) z^3 \log(z) + \frac{\sigma_s}{\zeta} z^3, \\ \chi_s(z \rightarrow z_h) &= c_{s,0} - \frac{(-2c_{s,0}^3 \lambda + 12c_{s,0} - \gamma c_{l,0}^2)}{16z_h} (z_h - z) + \mathcal{O}[(z_h - z)^2],\end{aligned}\tag{12}$$

Case II:

$$\begin{aligned}\chi_l(z \rightarrow 0) &= m_l \zeta z - \frac{\gamma}{4} m_l m_s \zeta^2 z^2 + \frac{m_l \zeta}{4} \left(4\mu_g^2 - 2\mu_c^2 + m_l^2 \zeta^2 \lambda - \frac{\gamma^2}{8} (m_l^2 \zeta^2 + m_s^2 \zeta^2) \right) z^3 \log(z) + \frac{\sigma_l}{\zeta} z^3, \\ \chi_l(z \rightarrow z_h) &= c_{l,0} - \frac{c_{l,0}(4\mu_c^2 z_h^2 - 2c_{l,0}^2 \lambda + 12 - \gamma c_{s,0})}{16z_h} (z_h - z) + \mathcal{O}[(z_h - z)^2],\end{aligned}\tag{13}$$

$$\begin{aligned}\chi_s(z \rightarrow 0) &= m_s \zeta z - \frac{\gamma}{4} m_l^2 \zeta^2 z^2 + \frac{1}{4} \left(4\mu_g^2 m_s \zeta - 2\mu_c^2 m_s \zeta + m_s^3 \zeta^3 \lambda - \frac{\gamma^2}{4} m_l^2 m_s \zeta^3 \right) z^3 \log(z) + \frac{\sigma_s}{\zeta} z^3, \\ \chi_s(z \rightarrow z_h) &= c_{s,0} - \frac{(4c_{s,0} \mu_c^2 z_h^2 - 2c_{s,0}^3 \lambda + 12c_{s,0} - \gamma c_{l,0}^2)}{16z_h} (z_h - z) + \mathcal{O}[(z_h - z)^2],\end{aligned}\tag{14}$$

where m_l and m_s are the light and strange quark masses, respectively, σ_l and σ_s are the chiral condensate of light and strange quark, $\zeta = \frac{\sqrt{N_c}}{2\pi}$ is a normalization factor which is fixed by matching the two point correlation function of the scalar operator with the 4D results [50], and $c_{l(s),0}$ is an integration constant.

III. MESON SUSCEPTIBILITY IN SOFT-WALL MODEL

We consider two models in our work, for which the mass spectra of the mesons are given in Ref. [37] for case I and Refs. [41, 51] for case II. Here, we focus on the chiral and $U(1)_A$ symmetry partners of the scalar and pseudoscalar mesons.

A. Scalar sector

For the scalar and pseudo-scalar mesons, the perturbations on the background have the following form,

$$X = (X_0 + S)e^{2i\pi},\tag{15}$$

with S representing scalar field fluctuation and π pseudoscalar field fluctuation. The scalar field is defined by a 3×3 matrix,

$$S = S^a t^a = \frac{1}{\sqrt{2}} \begin{pmatrix} \frac{a_0}{\sqrt{2}} + \frac{\sigma_8}{\sqrt{6}} + \frac{\sigma_0}{\sqrt{3}} & a^+ & \kappa^+ \\ a^- & -\frac{a_0}{\sqrt{2}} + \frac{\sigma_8}{\sqrt{6}} + \frac{\sigma_0}{\sqrt{3}} & \kappa^0 \\ \kappa^- & \bar{\kappa}^0 & -\frac{2\sigma_8}{\sqrt{6}} + \frac{\sigma_0}{\sqrt{3}} \end{pmatrix},\tag{16}$$

where $t^a = \lambda_a/2$ ($a = 0, 1, \dots, 8$) are the generators of $U(3)$, where $\lambda_{a=1, \dots, 8}/2$ are the Gell-Mann matrices with $\lambda_0 = \sqrt{2/3}\mathbf{1}_{3 \times 3}$. The σ_0 and σ_8 are referred to as the admixtures of the $f_0(500)$ and $f_0(980)$.

The effective action of the scalar fluctuation up to the second order is given by

$$S_S = \frac{1}{2} \int d^5x \sqrt{g} e^{-\Phi} [g^{\mu\nu} \partial_\mu S^a \partial_\nu S^b + g^{zz} (\partial_z S^a) (\partial_z S^b) - m_5^2 S^a S^b - M^{a,b}(z) S^a S^b], \quad (17)$$

where

$$\begin{aligned} M^{a,b}(z) &= \lambda M_s^{a,b}(z) + 2\gamma M_{det}^{a,b}(z), \\ M_s^{a,b}(z) &= 2Tr(\{t^a, X_0\}\{t^b, X_0\} + 2t^a t^b X_0 X_0), \end{aligned} \quad (18)$$

The non-zero values of the $M_s^{a,b}(z)$ and $M_{det}^{a,b}(z)$ are given in Appendix A. For the sake of convenience, One can transform the system from the coordinate space (x) to the momentum space (p) by taking the Fourier transformation $S^a(x, z) = \frac{1}{(2\pi)^4} \int d^4p e^{ip \cdot x} S^a(p, z)$. Here, we investigate the two-point correlation function and susceptibility of the $a_0(980)$ and $f_0(500)$ (σ) mesons in the scalar sector. First, let's consider the case of the $a_0(980)$ meson, where the flavor index $a = b = 1, 2$ or 3 . Then, one can obtain the EOM as follows

$$S^{a''} + \left(3A' + \frac{f'}{f} - \Phi'\right) S^{a'} - \left(\frac{p^2}{f} + \frac{m_5^2 + M^{a,a}(z)}{f} A'^2\right) S^a = 0. \quad (19)$$

It is worth mentioning that this equation can not be solved analytically. Therefore, we need a numerical technique, such as the shooting method, to solve the EOM with the constraints from the boundary and horizon. Substituting the value of $M^{3,3}(z)$, the equation of motion reduces to ²

$$S'' + \left(3A' + \frac{f'}{f} - \Phi'\right) S' - \left(\frac{p^2}{f} + \frac{4m_5^2 - \gamma\chi_s + 6\lambda\chi_l^2}{4f} A'^2\right) S = 0. \quad (20)$$

The asymptotic solution of the scalar field $S(p, z)$ near the UV boundary $z \rightarrow 0$ is obtained as

$$S(z \rightarrow 0) = s_1 z + \frac{\gamma}{4} \zeta m_s s_1 z^2 + s_3 z^3 - \frac{1}{32} [s_1 (16(-p^2 + \mu_c^2 - 2\mu_g^2) - 24\zeta^2 \lambda m_l^2) + s_1 \gamma^2 \zeta^2 m_s^2] z^3 \log(z) + \mathcal{O}(z^4), \quad (21)$$

where s_1 and s_3 are the integration constants. According to the holographic dictionary, s_1 corresponds to the external source J_S , and s_3 corresponds to the operator $\bar{q}q$. Near the horizon $z = z_h$, one can also get the non-singular solution as

$$S(z \rightarrow z_h) = s_{h0} - \frac{12 - 6c_{l,0}^2 \lambda + \gamma c_{s,0} - 4p^2 z_h^2 + 4\mu_c^2 z_h^2}{16z_h} s_{h0} (z_h - z) + \mathcal{O}[(z_h - z)^2], \quad (22)$$

where s_{h0} is another integration constant. The parameters $c_{l,0}$ and $c_{s,0}$ are the integration constants of the χ_l and χ_s at the horizon, which can be achieved by solving Eq. (10) numerically for different temperatures or z_h . Substituting EOM into the action, one can get the corresponding on-shell action as

$$S_{a_0}^{\text{on}} = -\frac{1}{2} \int d^4p f(z) S(-p, z) e^{3A(z) - \Phi(z)} S'(p, z) \Big|_{z=\epsilon}^{z=z_h}, \quad (23)$$

where ϵ is an UV cutoff regularizing the on-shell action. Finally, one can derive the two-point Green's function of the scalar meson by taking the second-order derivative of the on-shell action S_S^{on} with respect to the external source J_S

² We omitted the flavor index for simplicity.

$$G_{a_0}(p) = \frac{\delta^2 S_{a_0}^{\text{on}}}{\delta J_{a_0}^* \delta J_{a_0}} \Big|_{z=\epsilon} = -\frac{4s_3}{s_1} - \frac{3\gamma}{32}(\zeta m_s)^2 - \frac{3}{4}\zeta^2 \lambda m_l^2 + \frac{1}{2}(\mu_c^2 - 2\mu_g^2 - p^2) \quad (24)$$

The scalar susceptibility is defined by the two-point Green's function at zero momentum transfer,

$$\chi_{a_0} = -\lim_{p^2 \rightarrow 0} G_{a_0}(p) = -\lim_{p^2 \rightarrow 0} \frac{\delta^2 S_{a_0}^{\text{on}}}{\delta J_{a_0}^* \delta J_{a_0}} \Big|_{z=\epsilon} = \frac{4s_3}{s_1} + \frac{3\gamma}{32}(\zeta m_s)^2 + \frac{3}{4}\lambda \zeta^2 m_l^2 - \frac{1}{2}(\mu_c^2 - 2\mu_g^2) \quad (25)$$

We did the analysis for case II; however, to extend the following analysis to case I, remove μ_c and make the substitution $\mu_g^2 \rightarrow -\mu_1^2$ in Eqs. (22-26). This same transformation applies to all subsequent results.

The mass-like parameter $M^{a,b}(z)$ in Eq. (18) is non-diagonal, and there is a mixing between the singlet and octet states. In order to find the equation of motion for the physical states σ and $f_0(980)$, we need to diagonalize the mass term $M^{a,b}(z)$ by applying an orthogonal transformation in the following way [15]:

$$\begin{aligned} \tilde{S}^i &= O^{ia} S^a, \\ \tilde{M}^{i,j} &= O^{ia} (M^{a,b}) O^{bj}. \end{aligned} \quad (26)$$

The value of $M^{a,b}(z)$ for the singlet, octet states with their mixing are

$$\begin{aligned} M^{0,0} &= \lambda M_s^{0,0} + \gamma M_{det}^{0,0} = \frac{\lambda}{2}(2\chi_l^2 + \chi_s^2) + \frac{\gamma}{6}(2\chi_l + \chi_s), \\ M^{8,8} &= \lambda M_s^{8,8} + \gamma M_{det}^{8,8} = \frac{\lambda}{2}(\chi_l^2 + 2\chi_s^2) - \frac{\gamma}{12}(4\chi_l - \chi_s), \\ M^{0,8} &= \lambda M_s^{0,8} + \gamma M_{det}^{0,8} = \frac{\lambda}{2}(\chi_l^2 - \chi_s^2) - \frac{\gamma}{3\sqrt{2}}(4\chi_l - \chi_s). \end{aligned} \quad (27)$$

The corresponding mass like parameter for the physical states σ and $f_0(980)$ are obtained as

$$\begin{aligned} M_\sigma(z) &= M^{0,0}(z) \cos^2 \theta_S + M^{8,8}(z) \sin^2 \theta_S + 2M^{0,8}(z) \cos \theta_S \sin \theta_S, \\ M_{f_0(980)}(z) &= M^{0,0}(z) \sin^2 \theta_S + M^{8,8}(z) \cos^2 \theta_S - 2M^{0,8}(z) \cos \theta_S \sin \theta_S, \end{aligned} \quad (28)$$

where θ_S represents the scalar mixing angle,

$$\tan 2\theta_S(z) = \frac{2M^{0,8}(z)}{M^{0,0}(z) - M^{8,8}(z)}. \quad (29)$$

The difference between the mixing angle here with the conventional linear sigma model is that, the θ_S is a function of the holographic coordinate z . Now, we can obtain the equation of motion for σ from the action,

$$S_\sigma = \frac{1}{2} \int dx^5 \sqrt{g} e^{-\Phi} \left[g^{\mu\nu} \partial_\mu S \partial_\nu S + g^{zz} (\partial_z S)^2 - m_5^2 S^2 - M_\sigma(z) S^2 \right]. \quad (30)$$

$$S'' + \left(3A' + \frac{f'}{f} - \Phi' \right) S' - \left(\frac{p^2}{f} + \frac{m_5^2 + M_\sigma(z)}{f} A'^2 \right) S = 0 \quad (31)$$

Similar to the a_0 state, we can obtain the asymptotic solution for σ near the boundary and the horizon. The solution near boundary is obtained as

$$S(z \rightarrow 0) = s_1 z + s_1 s_\gamma z^2 - \frac{1}{2} s_1 (\mu_c^2 - 2\mu_g^2 - p^2 + s_\gamma^2 + s_\lambda) z^3 \log(z) + s_3 z^3 + \mathcal{O}(z^4), \quad (32)$$

where

$$\begin{aligned} s_\gamma &= \gamma\zeta \left(\frac{1}{12}(4m_l - m_s)(\sin\theta_S(\epsilon))^2 - \frac{1}{6}(2m_l + m_s)(\cos\theta_S(\epsilon))^2 + \frac{1}{3\sqrt{2}}(m_l - m_s)\sin\theta_S(\epsilon)\cos\theta_S(\epsilon) \right), \\ s_\lambda &= \lambda\zeta^2 \left(\frac{1}{2}(m_l^2 + 2m_s^2)(\sin\theta_S(\epsilon))^2 + \frac{1}{2}(2m_l^2 + m_s^2)(\cos\theta_S(\epsilon))^2 + \sqrt{2}(m_l^2 - m_s^2)\sin\theta_S(\epsilon)\cos\theta_S(\epsilon) \right). \end{aligned} \quad (33)$$

And near to the horizon, the solution is

$$S(z \rightarrow z_h) = s_{h0} - \frac{3 - M_\sigma(zh) - p^2 zh^2}{4z_h} s_{h0} (z_h - z) + \mathcal{O}[(z_h - z)^2]. \quad (34)$$

The two-point correlation function and the σ susceptibility obtained from the second-order functional derivative of the on-shell action for σ with respect to the source are as follows

$$G_\sigma(p) = \frac{\delta^2 S_\sigma^{\text{on}}}{\delta J_\sigma^* \delta J_\sigma} \Big|_{z=\epsilon} = -\frac{4s_3}{s_1} - 2s_\gamma^2 + \frac{1}{2}(\mu_c^2 - 2\mu_g^2 - p^2 + s_\gamma^2 + s_\lambda). \quad (35)$$

$$\chi_\sigma = -\lim_{p^2 \rightarrow 0} G_\sigma(p) = \frac{4s_3}{s_1} + 2s_\gamma^2 - \frac{1}{2}(\mu_c^2 - 2\mu_g^2 + s_\gamma^2 + s_\lambda). \quad (36)$$

B. Pseudoscalar channel

In this section, we investigate the two-point correlation function and susceptibilities of the pion and η particles. The pseudoscalar field is defined through the perturbation on the background as given by Eq. (15), where π is the pseudoscalar field and is given by

$$\pi = \pi^a t^a = \frac{1}{\sqrt{2}} \begin{pmatrix} \frac{\pi^0}{\sqrt{2}} + \frac{\eta_8}{\sqrt{6}} + \frac{\eta_0}{\sqrt{3}} & \pi^+ & K^+ \\ \pi^- & -\frac{\pi^0}{\sqrt{2}} + \frac{\eta_8}{\sqrt{6}} + \frac{\eta_0}{\sqrt{3}} & K^0 \\ K^- & \bar{K}^0 & -\frac{2\eta_8}{\sqrt{6}} + \frac{\eta_0}{\sqrt{3}} \end{pmatrix}, \quad (37)$$

where η^0 and η_8 are singlet and octet components of the pseudoscalar field and referred to as the mixing of the physical η and η' particles. It is worth mentioning that, the axial-vector field contributes to the pseudoscalar sectors and couples to the pion field.

The pion field and the longitudinal part (φ) of the axial-vector field are coupled in the pseudoscalar channel. The pion fluctuation becomes

$$\begin{aligned} S_\pi &= -\frac{1}{2g_5^2} \int d^5x \sqrt{g} e^{-\Phi} \sum_{i=1}^3 \left\{ g^{\mu\nu} g^{zz} \partial_z \partial_\mu \varphi^i \partial_z \partial_\nu \varphi^i - g_5^2 \chi_l^2 (g^{\mu\nu} \partial_\mu \varphi^i \partial_\nu \varphi^i \right. \\ &\quad \left. + g^{\mu\nu} \partial_\mu \pi^i \partial_\nu \pi^i + g^{zz} (\partial_z \pi^i)^2 - 2g^{\mu\nu} \partial_\mu \varphi^i \partial_\nu \pi^i \right\}. \end{aligned} \quad (38)$$

From the action, one can derive the EOMs for the pion field and the axial-vector field as

$$\begin{aligned} \varphi'' + \left(A' + \frac{f'}{f} - \Phi' \right) \varphi' - \frac{e^{2A} g_5^2 \chi_l^2}{f} (\varphi - \pi) &= 0, \\ \pi'' + \left(3A' + \frac{f'}{f} - \Phi' + \frac{2\chi_l'}{\chi_l} \right) \pi' + \frac{p^2}{f} (\varphi - \pi) &= 0. \end{aligned} \quad (39)$$

The asymptotic solutions of the EOMs for the pion field at the boundary can be easily derived as [45],

$$\begin{aligned}\varphi(z \rightarrow 0) &= c_f - \frac{1}{2}\zeta^2 g_5^2 m_l^2 \pi_0 z^2 \log(z) + \varphi_2 z^2 + \mathcal{O}(z^3), \\ \pi(z \rightarrow 0) &= \pi_0 + c_f + \frac{1}{2}\pi_0 p^2 z^2 \log(z) + \pi_2 z^2 + \mathcal{O}(z^3),\end{aligned}\tag{40}$$

where c_f, φ_2, π_0 , and π_2 are the integration constants. π_0 is identified as the external source J_π . It has been pointed out by the work of Ref. [52] that c_f is a redundant free parameter and can be set to zero for simplicity. On the other hand, we can also derive the boundary conditions at the horizon, which take the following forms,

$$\begin{aligned}\varphi(z \rightarrow z_h) &= -\frac{c_{l,0}^2 \pi^2}{z_h} \pi_{h0} (z_h - z) + \mathcal{O}\left[(z - z_h)^2\right], \\ \pi(z \rightarrow z_h) &= \pi_{h0} + \frac{p^2 z_h}{4} \pi_{h0} (z_h - z) - \mathcal{O}\left[(z - z_h)^2\right].\end{aligned}\tag{41}$$

Here, π_{h0} is another integration constant. The on-shell action of the pion part is

$$S_\pi^{\text{on}} = -\frac{1}{2g_5^2} \int d^4 p e^{A-\Phi} \left[e^{2A} g_5^2 f \chi_l^2 \pi(-p, z) \pi'(p, z) + p^2 f \varphi(-p, z) \varphi'(p, z) \right] \Bigg|_{z=\epsilon}^{z=z_h}.\tag{42}$$

From Eq. (39), we can find a first order differential equation for π and φ fields as

$$p^2 \partial_z \varphi + e^{2A(z)} g_5^2 \chi_l^2 \partial_z \pi = 0\tag{43}$$

Keeping in mind that, one can write the fields in holographic QCD as the source and the bulk-to-boundary propagator, we can write both π and φ near the boundary as

$$\begin{aligned}\varphi(z \rightarrow 0) &= \pi_0 \varphi_b = \pi_0 \left(-\frac{1}{2}\zeta^2 g_5^2 m_l^2 z^2 \log(z) + \frac{\varphi_2}{\pi_0} z^2 + \mathcal{O}(z^3) \right), \\ \pi(z \rightarrow 0) &= \pi_0 \pi_b = \pi_0 \left(1 + \frac{1}{2} p^2 z^2 \log(z) + \frac{\pi_2}{\pi_0} z^2 + \mathcal{O}(z^3) \right),\end{aligned}\tag{44}$$

where b refers to the bulk-to-boundary propagator. We may construct a solution of the pion field perturbatively in m_π by letting $\varphi_b(z) = a_1(0, z) - 1$ [28], where a_1 is the bulk-to-boundary propagator of the axial-vector field for the a_1 meson with $p^2 = 0$. Now, the on-shell action for the pion becomes

$$S_\pi^{\text{on}} = -\frac{1}{2g_5^2} \int d^4 p e^{A-\Phi} \left[-f m_\pi^2 \pi_b(-p, z) a_1'(0, z) + p^2 f \varphi_b(-p, z) \varphi_b'(p, z) \right] \Bigg|_{z=\epsilon}^{z=z_h},\tag{45}$$

where $m_\pi^2 = -\mathbf{p}^2$ is the screening mass of the pion. Now, before going to find the two-point correlation function, we need to find the solution of the a_1 field. Considering the gauge field in the action Eq. (4), we can obtain the axial-vector fluctuation of the a_1 particle as

$$\begin{aligned}S_{a_1} &= -\frac{1}{2g_5^2} \int d^5 x \sqrt{g} e^{-\Phi} \left\{ \sum_{i=1}^3 \left\{ g^{zz} g^{\mu\nu} \partial_z a_{1,\mu}^i \partial_z a_{1,\nu}^i + g^{\mu\nu} g^{mn} \partial_\mu a_{1,m}^i \partial_\nu a_{1,n}^i \right\} \right. \\ &\quad \left. - g_5^2 \chi^2 \sum_{i=1}^3 g^{mn} a_{1,m}^i a_{1,n}^i \right\}.\end{aligned}\tag{46}$$

With the equation of motion derived from the action

$$a_1'' + \left(A' + \frac{f'}{f} - \Phi' \right) a_1' - \frac{e^{2A} g_5^2 \chi^2 + p^2}{f} a_1 = 0.\tag{47}$$

Similarly, we obtain the UV boundary conditions for the bulk-to-boundary propagator of the axial-vector,

$$a_1(0, z \rightarrow 0) = 1 + \frac{a_{1,2}}{a_{1,0}} z^2 + \frac{1}{2} z^2 \log(z) [\zeta^2 g_5^2 m_l^2] + \mathcal{O}(z^3), \quad (48)$$

where $a_{1,0}$ (corresponds to the source of the axial-vector field) and $a_{1,2}$ are the integration constants. Inserting the asymptotic value of a_1 field into Eq. (45), one can obtain the two-point correlation function of the pion

$$G_\pi(p) = \frac{m_\pi^2}{2g_5^2} \left[\frac{2a_{1,2}}{a_{1,0}} + \frac{1}{2} (\zeta^2 g_5^2 m_l^2) \right]. \quad (49)$$

Then, following the standard definition of the susceptibility, we can obtain the pion susceptibility as

$$\chi_\pi = - \lim_{p^2 \rightarrow 0} G_\pi(p) = - \frac{m_\pi^2}{2g_5^2} \left[\frac{2a_{1,2}}{a_{1,0}} + \frac{1}{2} \zeta^2 g_5^2 m_l^2 \right]. \quad (50)$$

By using the definition of the pion decay constant in holographic QCD, $f_\pi^2 = -\frac{e^A}{g_5^2} a_1'(0, z)|_{z=\epsilon}$, we can see that the pion susceptibility is

$$\chi_\pi = \frac{1}{2} m_\pi^2 f_\pi^2. \quad (51)$$

From the dimensional analysis point of view, we can see that the mass dimension of χ_π is [4], which is higher than the actual mass dimension of the susceptibility, which is [2]. We can use another method to check the consistency of our method of deduction of the χ_π . By considering the Ward-Takahashi identity (WTI), the pion susceptibility χ_π can be derived from the QCD Lagrangian [16], which is given by

$$\chi_\pi = i \frac{\langle q\bar{q} \rangle}{m_l}, \quad (52)$$

By using the GOR relation $2m_l \langle q\bar{q} \rangle_l = m_\pi^2 f_\pi^2$, we can match Eq. (51) with the one found from the WTI in Eq. (52), and conclude that we need to normalize Eq. (51) with $1/(m_l^2)$,

$$\chi_\pi = \frac{1}{2m_l^2} m_\pi^2 f_\pi^2. \quad (53)$$

Similar to the scalar channel, there is a mixing between the singlet and octet channels of the pseudoscalar field. The action for the singlet and octet channels is given by

$$S_\pi = - \frac{1}{2g_5^2} \int d^5x \sqrt{g} e^{-\Phi} \left\{ \sum_{i,j=0,8} \left\{ g^{\mu\nu} g^{zz} \partial_z \partial_\mu \varphi^i \partial_z \partial_\nu \varphi^j - g_5^2 M_A^{i,j}(z) (g^{\mu\nu} \partial_\mu \varphi^i \partial_\nu \varphi^j + g^{\mu\nu} \partial_\mu \pi^i \partial_\nu \pi^j + g^{zz} \partial_z \pi^i \partial_z \pi^j - 2g^{\mu\nu} \partial_\mu \varphi^i \partial_\nu \pi^j) \right\} - g_5^2 \frac{3\gamma}{4} \chi_l^2 \chi_s \pi^0 \pi^0 \right\}. \quad (54)$$

where i and j take the values of 0 and 8, and $M_A^{i,j}(z)$ is defined by

$$M_A^{i,j}(z) = 2Tr(\{t^i, X_0\} \cdot \{t^j, X_0\}). \quad (55)$$

The mixing between $M_A^{0,0}(z)$ and $M_A^{8,8}(z)$ can be encountered by applying the orthogonal rotation such as

$$\begin{aligned} \tilde{\pi}^i &= O^{ia} \pi^a \\ \tilde{M}_A^{i,j} &= O^{ia} \left(M_A^{a,b} \right) O^{bj}. \end{aligned} \quad (56)$$

$$\begin{aligned}
M_A^{0,0}(z) &= \frac{1}{3}(2\chi_l^2(z) + \chi_s^2(z)) \\
M_A^{8,8} &= \frac{1}{3}(\chi_l^2(z) + 2\chi_s^2(z)) \\
M_A^{0,8} &= \frac{\sqrt{2}}{3}(\chi_l^2(z) - \chi_s^2(z))
\end{aligned} \tag{57}$$

The mass term for the physical η and η' states are become

$$\begin{aligned}
M_{\eta'}(z) &= M_A^{0,0}(z) \cos^2 \theta_p + M_A^{8,8}(z) \sin^2 \theta_p + 2M_A^{0,8}(z) \cos \theta_p \sin \theta_p, \\
M_{\eta}(z) &= M_A^{0,0}(z) \sin^2 \theta_p + M_A^{8,8}(z) \cos^2 \theta_p - 2M_A^{0,8}(z) \cos \theta_p \sin \theta_p,
\end{aligned} \tag{58}$$

where $\theta_p(z)$ is the pseudoscalar mixing angle given by

$$\tan 2\theta_p(z) = \frac{2M_A^{0,8}(z)}{M_A^{0,0}(z) - M_A^{8,8}(z)}. \tag{59}$$

It is worth noting that in Eq. (54), only the singlet state contribute to the determinant term, and after applying the orthogonal transformation, there is a mixing term between η and η' states which results in a coupled equation of motions for them. The equation of motion for η and η'

$$\begin{aligned}
\varphi''_{\eta} + \left(A' + \frac{f'}{f} - \Phi' \right) \varphi'_{\eta} - \frac{e^{2A} g_5^2 M_{\eta}(z)}{f} (\varphi_{\eta} - \pi_{\eta}) &= 0, \\
\pi''_{\eta} + \left(3A' + \frac{f'}{f} - \Phi' + \frac{(M_{\eta})'(z)}{M_{\eta}(z)} \right) \pi'_{\eta} + \frac{p^2}{f} (\varphi_{\eta} - \pi_{\eta}) + \frac{3e^{2A} \gamma}{4M_{\eta}(z)f} \chi_l^2 \chi_s (\pi_{\eta} \sin^2 \theta_p(z) - \pi_{\eta'} \sin \theta_p(z) \cos \theta_p(z)) &= 0.
\end{aligned} \tag{60}$$

$$\begin{aligned}
\varphi''_{\eta'} + \left(A' + \frac{f'}{f} - \Phi' \right) \varphi'_{\eta'} - \frac{e^{2A} g_5^2 M_{\eta'}(z)}{f} (\varphi_{\eta'} - \pi_{\eta'}) &= 0, \\
\pi''_{\eta'} + \left(3A' + \frac{f'}{f} - \Phi' + \frac{(M_{\eta'})'(z)}{M_{\eta'}(z)} \right) \pi'_{\eta'} + \frac{p^2}{f} (\varphi_{\eta'} - \pi_{\eta'}) + \frac{3e^{2A} \gamma}{4M_{\eta'}(z)f} \chi_l^2 \chi_s (\pi_{\eta'} \cos^2 \theta_p(z) - \pi_{\eta} \sin \theta_p(z) \cos \theta_p(z)) &= 0.
\end{aligned} \tag{61}$$

The expansion of the pseudoscalar field and the longitudinal part of the axial-vector field near the boundary is obtained as follows

$$\begin{aligned}
\varphi_{\eta}(z \rightarrow 0) &= c_f - \frac{1}{2} g_5^2 M_{\eta}(\epsilon) \pi_{\eta,0} z^2 \log(z) + \varphi_{\eta,2} z^2 + \mathcal{O}(z^3), \\
\pi_{\eta}(z \rightarrow 0) &= \pi_{\eta,0} + c_f + \pi_{\eta,1} z + \\
\frac{1}{2} \left(\pi_0 p^2 - \left(\frac{3\gamma \zeta^3 m_l^2 m_s}{4M_{\eta}(\epsilon)} \right) (\pi_{\eta,1} \sin^2 \theta_p(\epsilon) - \pi_{\eta',1} \cos \theta_p(\epsilon) \sin \theta_p(\epsilon)) \right) z^2 \log(z) &+ \pi_{\eta,2} z^2 + \mathcal{O}(z^3),
\end{aligned} \tag{62}$$

$$\begin{aligned}
\varphi_{\eta'}(z \rightarrow 0) &= c_f - \frac{1}{2} g_5^2 M_{\eta}(\epsilon) \pi_{\eta',0} z^2 \log(z) + \varphi_{\eta',2} z^2 + \mathcal{O}(z^3), \\
\pi_{\eta'}(z \rightarrow 0) &= \pi_{\eta',0} + c_f + \pi_{\eta',1} z + \\
\frac{1}{2} \left(\pi_0 p^2 - \left(\frac{3\gamma \zeta^3 m_l^2 m_s}{4M_{\eta'}(\epsilon)} \right) (\pi_{\eta',1} \cos^2 \theta_p(\epsilon) - \pi_{\eta,1} \cos \theta_p(\epsilon) \sin \theta_p(\epsilon)) \right) z^2 \log(z) &+ \pi_{\eta',2} z^2 + \mathcal{O}(z^3),
\end{aligned} \tag{63}$$

where

$$\pi_{\eta,1} = \frac{-1}{p^2 + 2\mu_g^2} \frac{3\gamma\zeta^3 m_l^2 m_s}{4M_\eta(\epsilon)} (\pi_{\eta,2} \sin^2 \theta_p(\epsilon) - \pi_{\eta',2} \cos \theta_p(\epsilon) \sin \theta_p(\epsilon)) \quad (64)$$

$$\pi_{\eta',1} = \frac{-1}{p^2 + 2\mu_g^2} \frac{3\gamma\zeta^3 m_l^2 m_s}{4M_{\eta'}(\epsilon)} (\pi_{\eta',2} \cos^2 \theta_p(\epsilon) - \pi_{\eta,2} \cos \theta_p(\epsilon) \sin \theta_p(\epsilon)) \quad (65)$$

Meanwhile, the non-singular solutions near the horizon are

$$\begin{aligned} \varphi_\eta(z \rightarrow z_h) &= -\frac{\pi^2 M_\eta(zh)}{z_h} \pi_{\eta,h0} (z_h - z) + \mathcal{O}[(z - z_h)^2], \\ \pi_\eta(z \rightarrow z_h) &= \pi_{\eta,h0} - \frac{\pi_{\eta,h0} zh}{4} \left(p^2 - \frac{3\gamma c_{l,0}^2 c_{s,0}}{4M_\eta(zh)zh^2} \left(\sin^2 \theta_p(zh) - \frac{\pi_{\eta',h0}}{\pi_{\eta,h0}} \sin \theta_p(zh) \cos \theta_p(zh) \right) \right) (z_h - z) + \mathcal{O}[(z - z_h)^2]. \end{aligned} \quad (66)$$

$$\begin{aligned} \varphi_{\eta'}(z \rightarrow z_h) &= -\frac{\pi^2 M_{\eta'}(zh)}{z_h} \pi_{\eta',h0} (z_h - z) + \mathcal{O}[(z - z_h)^2], \\ \pi_{\eta'}(z \rightarrow z_h) &= \pi_{\eta',h0} - \frac{\pi_{\eta',h0} zh}{4} \left(p^2 - \frac{3\gamma c_{l,0}^2 c_{s,0}}{4M_{\eta'}(zh)zh^2} \left(\cos^2 \theta_p(zh) - \frac{\pi_{\eta,h0}}{\pi_{\eta',h0}} \sin \theta_p(zh) \cos \theta_p(zh) \right) \right) (z_h - z) + \mathcal{O}[(z - z_h)^2]. \end{aligned} \quad (67)$$

After finding the on-shell action and taking the second-order functional derivative with respect to the source, one can obtain the two-point Green's function. Finally, the η susceptibility is given by the two-point Green's function at zero momentum transfer as mentioned earlier

$$\chi_\eta = -\lim_{p^2 \rightarrow 0} G_\eta(p) = -\frac{M_\eta(\epsilon)}{2g_s^2 \pi_{\eta,0} \pi_{\eta,0}} \left[\pi_{\eta,1}^2 - \pi_{\eta,0} \left(\frac{3\gamma\zeta^3 m_l^2 m_s}{4M_\eta(\epsilon)} \right) (\pi_{\eta,1} \sin^2 \theta_p(\epsilon) - \pi_{\eta',1} \cos \theta_p(\epsilon) \sin \theta_p(\epsilon)) + 2\pi_{\eta,0} \pi_{\eta,2} \right]. \quad (68)$$

Remark: The χ_η includes the contribution of both light and strange quarks. However, only the light quark component contributes to the study of $SU(2)$ chiral symmetry restoration and $U(1)_A$ symmetry restoration. Therefore, we can decompose the singlet and octet states of the pseudoscalar field in terms of the quark states as follows:

$$\begin{aligned} \pi^0 &= \frac{1}{\sqrt{3}}(u\bar{u} + d\bar{d} + s\bar{s}) = \frac{\sqrt{2}}{\sqrt{3}}\pi^l + \frac{1}{\sqrt{3}}\pi^s, \\ \pi^8 &= \frac{1}{\sqrt{6}}(u\bar{u} + d\bar{d} - 2s\bar{s}) = \frac{1}{\sqrt{3}}\pi^l - \frac{\sqrt{2}}{\sqrt{3}}\pi^s, \end{aligned} \quad (69)$$

where

$$\begin{aligned} \pi^l &= \frac{1}{\sqrt{2}}(u\bar{u} + d\bar{d}), \\ \pi^s &= s\bar{s}. \end{aligned} \quad (70)$$

We can express this decomposition in the language of orthogonal transformation as

$$\begin{pmatrix} \pi^8 \\ \pi^0 \end{pmatrix} = \begin{pmatrix} \cos \phi & -\sin \phi \\ \sin \phi & \cos \phi \end{pmatrix} \begin{pmatrix} \pi^l \\ \pi^s \end{pmatrix}, \quad (71)$$

where $\phi = 54.7^\circ$. Now one can write the mass term for the light and strange quark components as

$$\begin{aligned}
M_{\pi^i}(z) &= M_A^{8,8}(z) \cos^2 \phi + M_A^{0,0}(z) \sin^2 \phi + 2M_A^{0,8}(z) \cos \phi \sin \phi, \\
M_{\pi^s}(z) &= M_A^{8,8}(z) \sin^2 \phi + M_A^{0,0}(z) \cos^2 \phi - 2M_A^{0,8}(z) \cos \phi \sin \phi.
\end{aligned} \tag{72}$$

The steps of deriving the η_l susceptibility are similar to χ_η . The χ_{η_l} is given by

$$\chi_{\eta_l} = - \lim_{p^2 \rightarrow 0} G_{\eta_l}(p) = - \frac{M_{\pi^i}(\epsilon)}{2g_5^2 \pi_{\eta_l,0} \pi_{\eta_l,0}} \left[\pi_{\eta_l,1}^2 - \pi_{\eta_l,0} \left(\frac{3\gamma\zeta^3 m_l^2 m_s}{4M_{\pi^i}(\epsilon)} \right) (\pi_{\eta_l,1} \sin^2 \phi + \pi_{\eta^s,1} \cos \phi \sin \phi) + 2\pi_{\eta_l,0} \pi_{\eta_l,2} \right], \tag{73}$$

with

$$\pi_{\eta_l,1} = \frac{-1}{2\mu_g^2} \frac{3\gamma\zeta^3 m_l^2 m_s}{4M_{\pi^i}(\epsilon)} (\pi_{\eta_l,2} \sin^2 \phi + \pi_{\eta^s,2} \cos \phi \sin \phi) \tag{74}$$

$$\pi_{\eta^s,1} = \frac{-1}{2\mu_g^2} \frac{3\gamma\zeta^3 m_l^2 m_s}{4M_{\pi^s}(\epsilon)} (\pi_{\eta^s,2} \cos^2 \phi + \pi_{\eta_l,2} \cos \phi \sin \phi). \tag{75}$$

Keeping in mind that the normalization factor we have found for the pion susceptibility must be added to all pseudoscalar channels, including the η susceptibility.

IV. TOPOLOGICAL SUSCEPTIBILITY

The topological susceptibility is a quantity measuring the topological charge fluctuation of the QCD- θ vacuum, which is defined as the curvature of the θ -dependent QCD vacuum energy $V(\theta)$ at $\theta = 0$ [14],

$$\chi_{\text{top}} = - \int_T d^4x \frac{\delta^2 V(\theta)}{\delta\theta(x)\delta\theta(0)} \Big|_{\theta=0} \tag{76}$$

$V(\theta)$ represents the effective potential of QCD, which includes the QCD θ -term represented by the flavor-singlet gluonic operator. Since adding the $V(\theta)$ in holographic QCD is not straightforward, we will use the final form of the topological susceptibility expressed by fermionic operators as [16]

$$\chi_{\text{top}} = -\frac{1}{4} [m_l \langle \bar{\psi}\psi \rangle + im_l^2 \chi_{\eta_l}]. \tag{77}$$

By using Eq. (52), the topological susceptibility is written in terms of the pion susceptibility and light quark components of the η susceptibility, and it is proportional to the square of light quark mass,

$$\chi_{\text{top}} = \frac{im_l^2}{4} [\chi_\pi - \chi_{\eta_l}]. \tag{78}$$

To facilitate an understanding of the role of topological susceptibility, we insert the scalar meson susceptibilities χ_σ and χ_{a_0} in Eq. (78),

$$\begin{aligned}
\chi_{\text{top}} &= \frac{im_l^2}{4} [(\chi_\pi - \chi_\sigma) - (\chi_\eta - \chi_\sigma)] \\
\chi_{\text{top}} &= \frac{im_l^2}{4} [(\chi_\pi - \chi_{a_0}) - (\chi_\eta - \chi_{a_0})]
\end{aligned} \tag{79}$$

Writing the χ_{top} in this form, one can realize that the topological susceptibility is described by the combinations of the chiral partner $\chi_\pi \leftrightarrow \chi_\sigma$ ($\chi_{a_0} \leftrightarrow \chi_{\eta_l}$) and the $U(1)_A$ partner $\chi_\pi \leftrightarrow \chi_{a_0}$ ($\chi_{\eta_l} \leftrightarrow \chi_\sigma$). After the chiral restoration, the topological susceptibility is dominated by the $U(1)_A$ partner: $\chi_{\text{top}} \sim \chi_{\eta_l} - \chi_\sigma$ ($\chi_{\text{top}} \sim \chi_\pi - \chi_{a_0}$), so that χ_{top} acts as the indicator for the breaking strength of $U(1)_A$ symmetry. It should be noted that χ_{top} trivially vanishes in the chiral limit ($m_l = 0$). In this limit, the topological susceptibility is no longer considered an indicator.

$m_l = 7.5 \text{ MeV}$ ($m_\pi = 132.5 \text{ MeV}$)	$m_l = 13 \text{ MeV}$ ($m_\pi = 174.4 \text{ MeV}$)	$m_s = 95 \text{ MeV}$	$\mu_g = 0.44 \text{ (GeV)}$
$\mu_1 = 0.81 \text{ (GeV)}$	$\mu_2 = 0.176 \text{ (GeV)}$	$\lambda = 80$	$\gamma = -10$

TABLE I: The values of the free parameters for case I.

$m_l = 3.22 \text{ MeV}$ ($m_\pi = 141.6 \text{ MeV}$)	$m_l = 6 \text{ MeV}$ ($m_\pi = 193 \text{ MeV}$)	$m_s = 95 \text{ MeV}$	$\mu_g = 0.44 \text{ (GeV)}$
$\mu_c = 1.27 \text{ (GeV)}$	$\lambda = 80$	$\gamma = -23$	

TABLE II: The values of the free parameters for case II.

V. RESULTS

The objective of this work is to examine the restoration of chiral symmetry and $U(1)_A$ symmetry at finite temperature by analyzing the screening mass and meson susceptibility using the soft-wall holographic QCD model. As mentioned earlier, we consider two cases with different forms for the 5D mass and dilaton field. The parameters for cases I and II can be found in Table I and Table II, respectively. These parameters are chosen to achieve a physical pion mass and a pseudocritical temperature of approximately 155 MeV for both cases.

First, we discuss the chiral phase transition at physical quark masses with three-quark flavors. In Fig. 1, we present the light quark condensate σ_l and σ_s as functions of temperature for the three-quark flavor system with physical quark masses in case I. The left panel demonstrates that the chiral condensate σ_l smoothly decreases with increasing temperature, but does not reach zero even at high temperatures. This indicates that the holographic QCD model undergoes a chiral crossover, and chiral symmetry is approximately restored at finite temperatures. The chiral crossover is characterized by the pseudocritical temperature, which is determined by the inflection point of the quark condensate, $d^2\sigma_l/d^2T|_{T=T_{pc}} = 0$, and is evident as a peak in $d\sigma_l/dT$ as shown in the right panel of Fig. 1. The strange quark condensate exhibits similar behavior, with a higher value at high temperatures compared to the light quark condensate. For the three-quark flavor system with physical masses of light and strange quarks, the pseudocritical temperature is determined to be $T_{pc}|_{\text{hQCD}} = 0.157 \text{ GeV}$. A similar result for case II is shown in Fig. 2, where the pseudocritical temperature is determined to be $T_{pc}|_{\text{hQCD}} = 0.154 \text{ GeV}$.

A. Screening mass

In a vacuum, mesons are characterized by their masses and decay widths in different channels. At finite temperature, the concept of mass is replaced by screening mass and pole mass due to the breaking of Lorentz symmetry. Both of these masses carry information about the correlation function of the meson field in a hot medium. The screening mass, which can be evaluated as the pole of the spatial component of the two-point correlation function, serves as an indication of chiral symmetry restoration. This is because the mass difference of chiral partner mesons (π and σ , and η and a_0) originates from the spontaneous chiral symmetry breaking of QCD. After the chiral symmetry restoration,

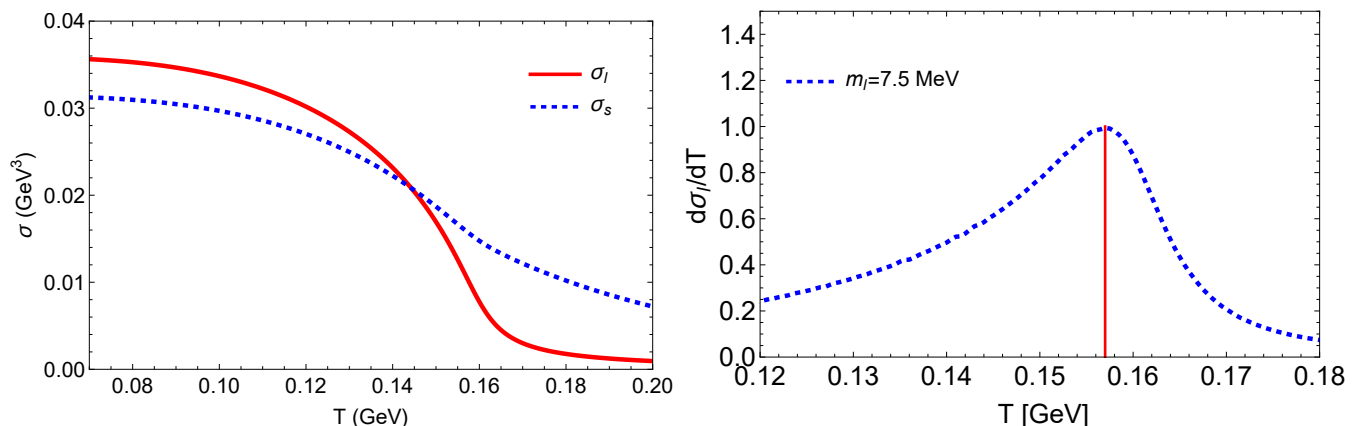


FIG. 1: Left: The light quark condensate σ_l and the strange quark condensate σ_s as functions of temperature T . Right: Evaluating the pseudocritical temperature at $T_{pc} = 0.157 \text{ GeV}$ from the peak of $d\sigma_l/dT$. These results are for case I with $m_l = 7.5 \text{ MeV}$.

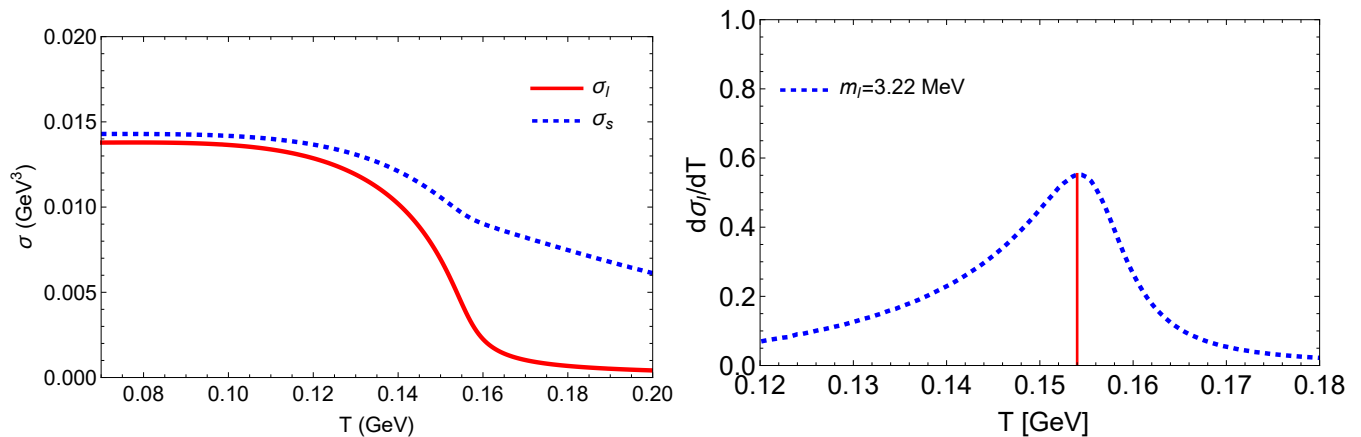


FIG. 2: The color online is similar to Fig. 1. The evaluated pseudocritical temperature is $T_{pc} = 0.154$ GeV with the case II parameter setup.

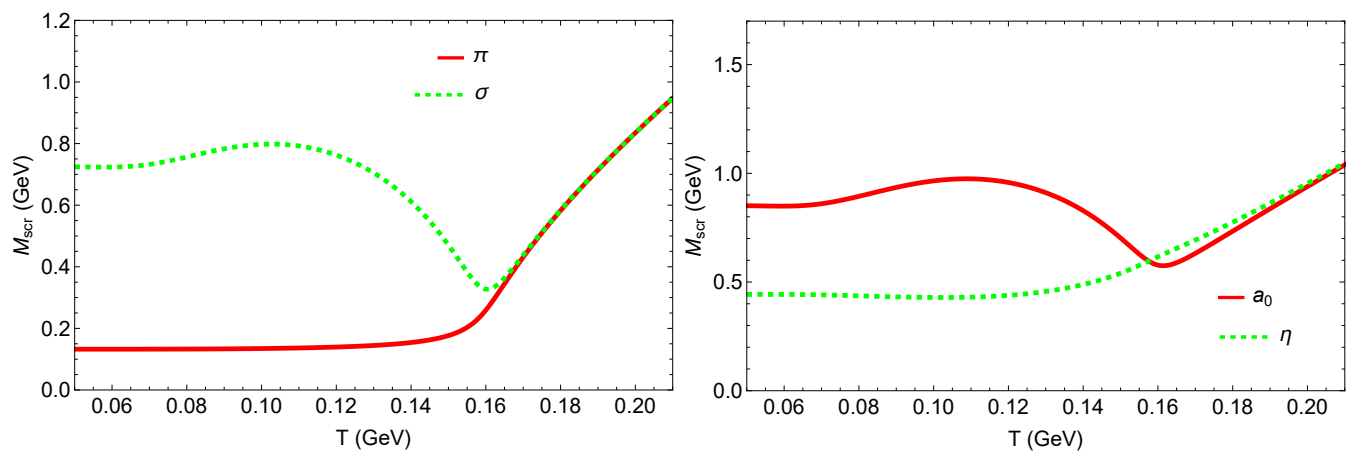


FIG. 3: Screening mass of the chiral symmetry partners (π and σ , and η and a_0) as a function of temperature for case I.

the masses of chiral partners should be degenerate.

In our work, we calculated the two-point Green's function for a_0 , σ , π , and η fields. The screening mass of the a_0 meson is obtained as the pole of G_{a_0} in Eq. (24), similar to the condition of $s_1(p^2) = 0$, which corresponds to the pole of G_{a_0} . The smallest spatial value of p^2 satisfying the condition $s_1(p^2) = 0$ is equal to the screening mass of a_0 , $M_{a_0,scr}^2 = -p^2$. Similarly, we can find the screening mass of the σ meson.

For the pseudoscalar sector, we need to follow the same method and find the pole of the two-point Green's functions, which correspond to the conditions $\pi_0(p^2) = 0$ and $\pi_{\eta,0}(p^2) = 0$ for the screening mass of the pion and η , respectively. The results of the screening masses of the chiral partners are shown in Fig. 3 and Fig. 4 for case I and case II, respectively. From these figures, we can see that near the pseudocritical temperature, the masses of chiral partners become degenerate, providing a signal of the chiral symmetry restoration. Quantitatively, these results are consistent with the ones present from LQCD [53] and Nambu-Jona-Lasinio (NJL) [54], and confirm that the temperature-dependent behavior of screening masses of the chiral partner mesons is strongly coupled with the chiral phase transition.

B. Meson susceptibility

In the study of symmetry restoration (chiral symmetry and $U(1)_A$ symmetry), an important indicator is the meson susceptibility, which measures the response of the system to the addition of a field. As demonstrated in the previous section, the pion susceptibility requires a normalization factor to align with the one obtained from the WTI. Similarly, for the σ susceptibility, a direct method can be used to determine χ_σ by taking the derivative of the chiral condensate with respect to the light quark mass:

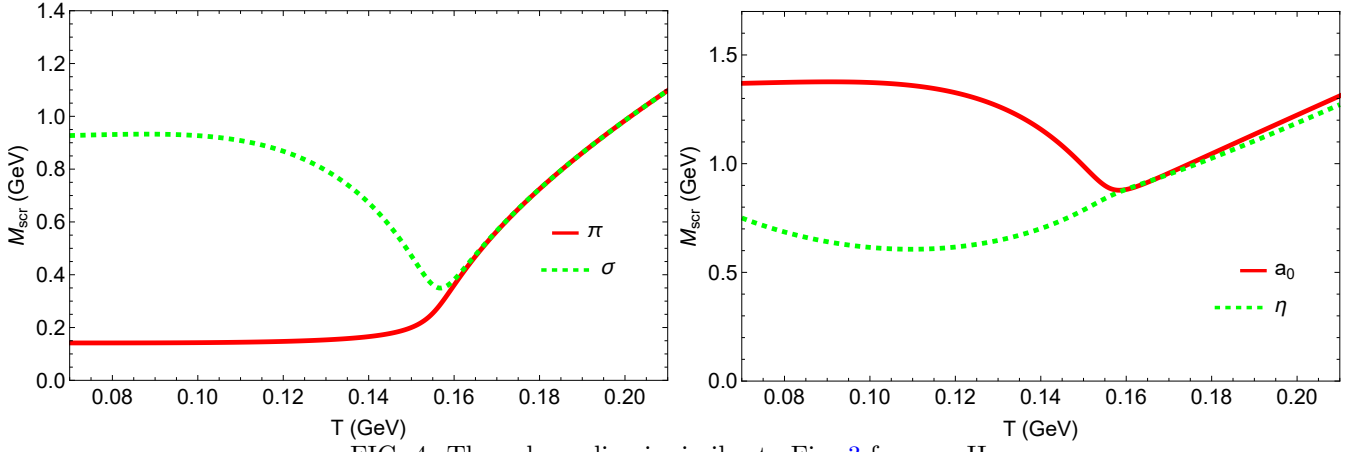


FIG. 4: The color online is similar to Fig. 3 for case II.

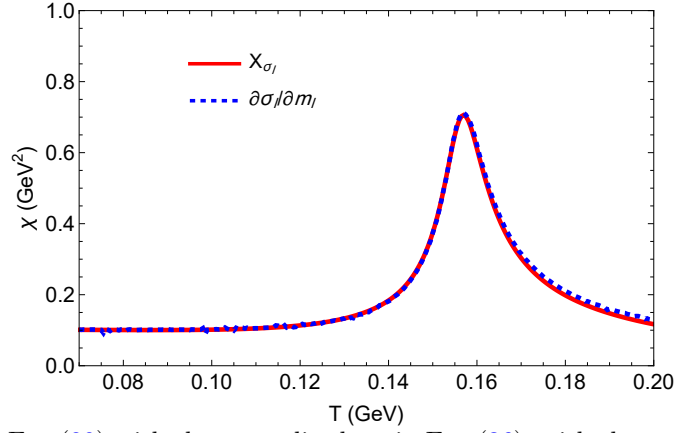


FIG. 5: Comparison of χ_σ in Eq. (80) with the normalized χ_σ in Eq. (36), with the normalization factor $N_\sigma = \zeta^2/4$.

$$\chi_\sigma = \frac{\partial\sigma_l}{\partial m_l}. \quad (80)$$

To relate the present definition of the susceptibility to the one given in Eq. (36), note that the two expressions differ only by an overall normalisation factor $\zeta^2/4$. A small deviation to the quark mass $m_l + \delta m_l$ will cause a small deviation $\delta\chi_l$ to χ_l . Obviously, the linearised fluctuation $\delta\chi$ obeys the same equation of motion as Eq. (31) evaluated at zero four-momentum, $p^2 = 0$. Therefore, the UV expansion of $\delta\chi_l$ should be $\delta\chi_l = s_1 z + \dots + s_3 z^3 + \dots$. On the other hand, the dual field-theory interpretation identifies the leading and sub-leading coefficients with the quark-mass and condensate variations: $s_1 = \delta m_l \zeta$ and $s_3 = \delta\sigma/\zeta$, and the susceptibility defined in Eq. (36) is therefore $\chi_\sigma \sim 4s_3/s_1 = 4(\delta\sigma/\zeta)/(\delta m_l \zeta) = \frac{4}{\zeta^2} \frac{\partial\sigma}{\partial m_l}$.

In Fig. 5, we compare the numerical results of χ_σ in Eq. (80) with the normalized χ_σ in Eq. (36). The normalization factor, found by equating Eq. (80) and Eq. (36), is $N_\sigma = \zeta^2/4$, which aligned with the normalization factor we obtained analytically.

Similar to the concept of screening mass, when two mesons are symmetry partners, their susceptibilities should be equal after symmetry restoration. The sign of chiral symmetry restoration can be observed in the following conditions.

$$\begin{aligned} \chi_\pi - \chi_\sigma &\rightarrow 0, \\ \chi_{\eta_l} - \chi_{a_0} &\rightarrow 0. \end{aligned} \quad (81)$$

Similarly, the indication of $U(1)_A$ symmetry restoration can be read from

$$\begin{aligned} \chi_\pi - \chi_{a_0} &\rightarrow 0, \\ \chi_{\eta_l} - \chi_\sigma &\rightarrow 0. \end{aligned} \quad (82)$$

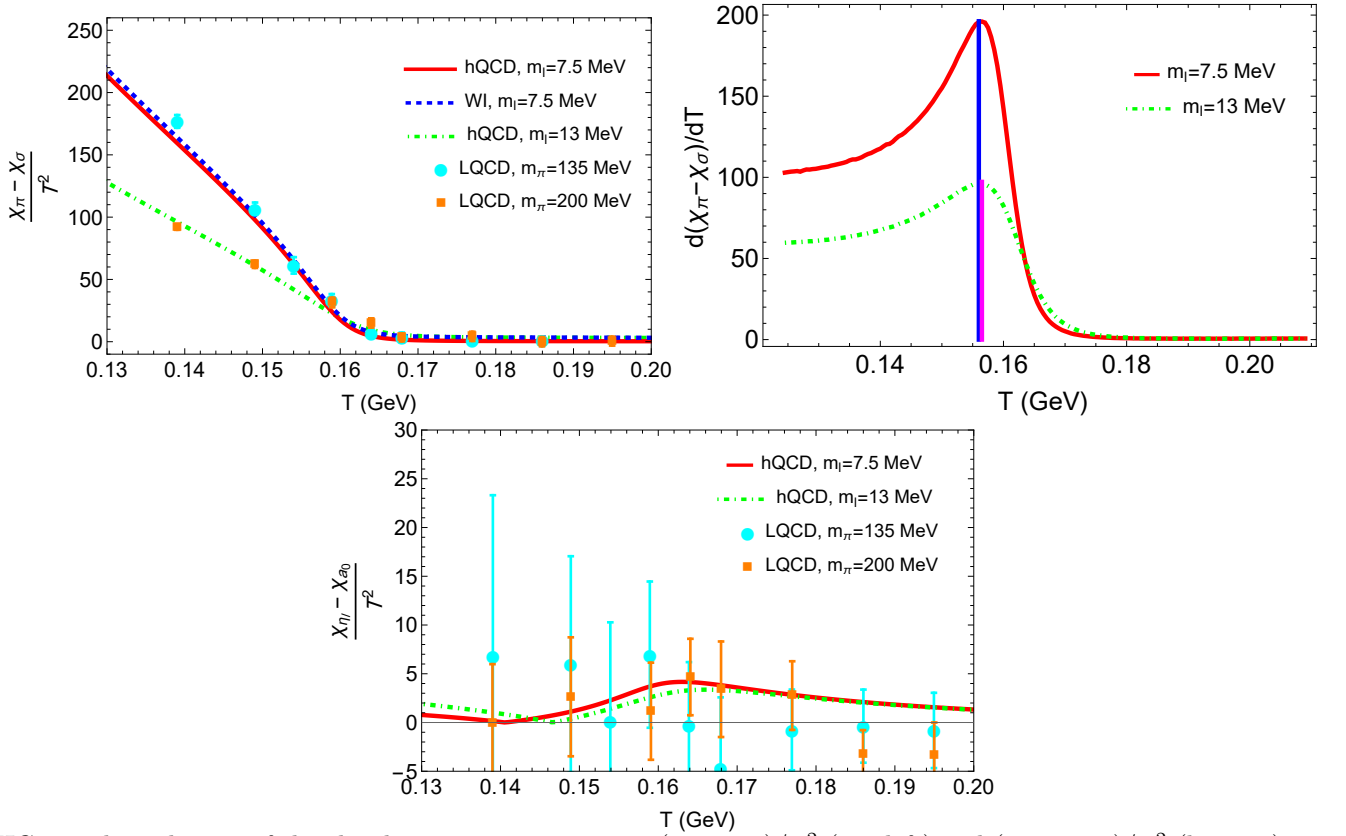


FIG. 6: The indicator of the chiral symmetry restoration $(\chi_\pi - \chi_\sigma)/T^2$ (top-left) and $(\chi_\eta - \chi_{a_0})/T^2$ (bottom) as a function of temperature at $m_l = 7.5$ MeV and $m_l = 13$ MeV for case I. The LQCD data is taken from Ref. [6].

The results of the $\chi_\pi - \chi_\sigma$ and $\chi_\eta - \chi_{a_0}$ as a function of temperature are shown in Fig. 6 and Fig. 7 for case I and case II, respectively. As shown in the top-left panel of Fig. 6, the indicator $(\chi_\pi - \chi_\sigma)/T^2$ for the isoscalar partners (σ , π) drops sharply near the crossover temperature, signaling the rapid restoration of chiral symmetry. This behavior is observed for both light quark masses $m_l = 7.5$ MeV and $m_l = 13$ MeV in our model and is consistent with the observation in lattice LQCD data at physical quark masses [6]. The pseudocritical temperature estimated, from the top-right panel of Fig. 6, is similar to the one found from Fig. 1, confirming the restoration of the chiral symmetry from the meson susceptibility.

The bottom panel of Fig. 6 displays the susceptibility difference of isovector partners a_0 and η_l at light quark masses $m_l = 7.5$ MeV and $m_l = 13$ MeV. Despite the higher restoration point compared to the isoscalar partners, the results are compatible with the LQCD data within the uncertainty. The discrepancy in the restoration temperatures between the two chiral partner pairs is a direct signature of the influential role played by the $U(1)_A$ anomaly. The η meson receives a significant mass contribution from the anomaly, which is reflected in its susceptibility. Therefore, for the susceptibilities of the isovector pair to become degenerate, it is not sufficient for the chiral condensate to melt; the effects of the $U(1)_A$ anomaly must also be sufficiently suppressed.

For case II (Fig. 6), the behavior of $\chi_\pi - \chi_\sigma$ qualitatively agrees with LQCD, and $\chi_\eta - \chi_{a_0}$ is compatible with LQCD for both $m_l = 3.22$ MeV and $m_l = 6$ MeV. The pseudocritical temperature evaluated for case II is also consistent with Fig. 2.

In order to identify the breaking of the $U(1)_A$ symmetry, we analyze the difference between the susceptibilities of the $U(1)_A$ symmetry partners π and a_0 ($\chi_\pi - \chi_{a_0}$), which is non-zero only when the $U(1)_A$ symmetry is explicitly broken by the anomaly, and it vanishes upon the effective restoration of anomaly, as displayed in Fig. 8 and Fig. 9 for cases I and II, respectively. Unlike the results for chiral symmetry restoration, the outcomes in Fig. 8 do not align with the LQCD data at the low and mid temperatures. However, the restoration temperature of the $U(1)_A$ symmetry is aligned with LQCD, which is located near $T \sim 0.190$ GeV. The degeneracy of the results for $m_l = 7.5$ MeV and $m_l = 13$ MeV for $T > 0.165$ GeV proves that the non-zero value of the $\chi_\pi - \chi_{a_0}$ comes from the axial anomaly, not the small quark mass. This indicates that, within our current holographic construction, the dynamics driving the chiral transition are different from those controlling the axial anomaly strength, which signals the emergence of two distinct energy scales.

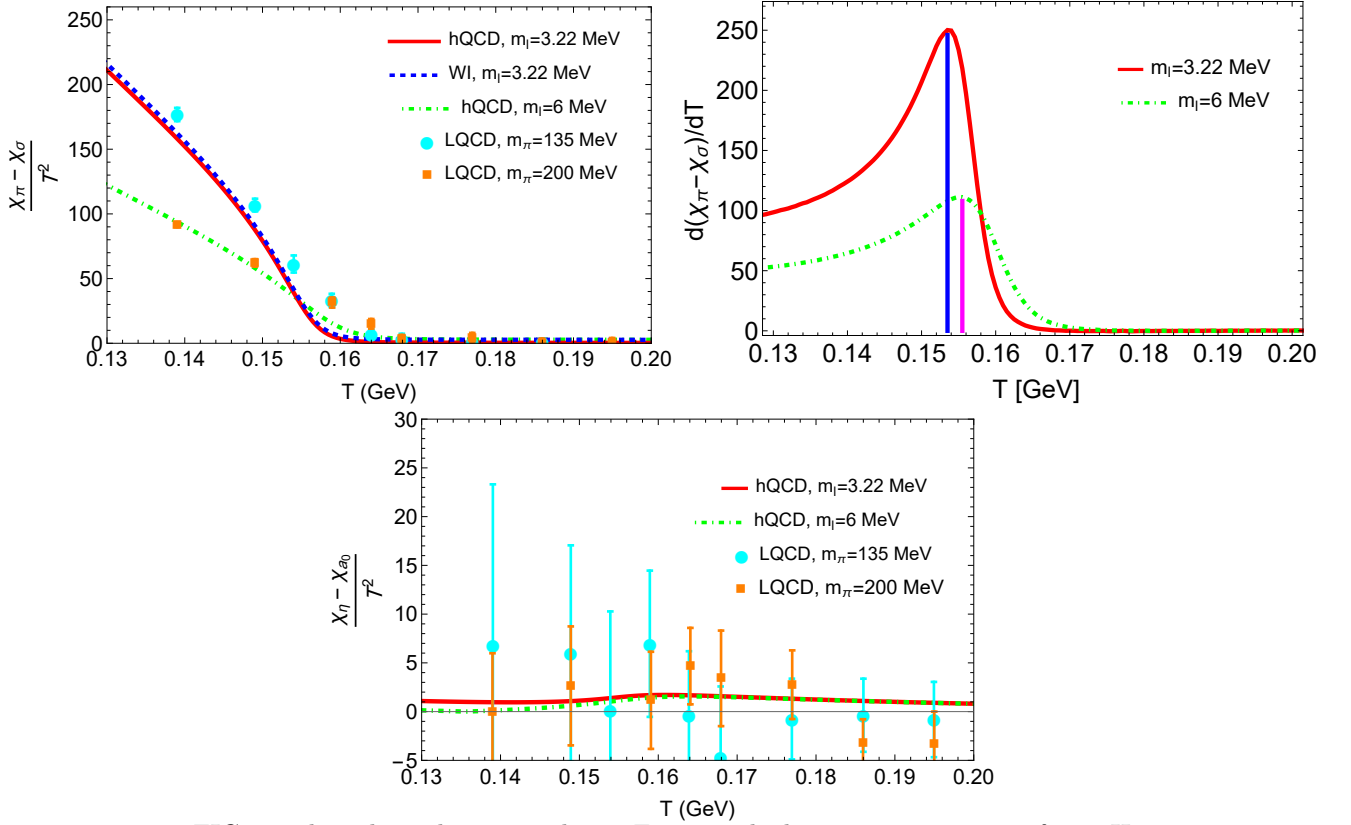


FIG. 7: The color online is similar to Fig. 6 with the parameterization of case II

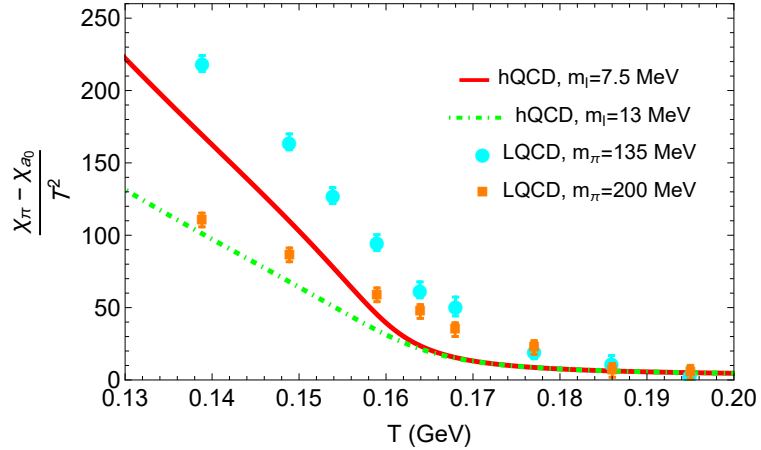


FIG. 8: The indicator of $U(1)_A$ symmetry breaking as a function of temperature at $m_l = 7.5$ MeV and $m_l = 13$ MeV. The susceptibilities difference, $\chi_\pi - \chi_{a_0}$, becomes quark mass independent for $T > 0.165$ GeV. These results are for case I. The LQCD data is taken from Ref. [6]

The situation described for Case I is found to be robust and is replicated in the alternative parameter set, Case II. As shown in Fig. 9, the $U(1)_A$ breaking indicator for Case II also undergoes its most rapid change at a temperature that coincides with the chiral pseudo-critical temperature for this situation. The restoration temperature, similar to case I, is $T \sim 0.190$ GeV. Then, within the holographic QCD, the restoration point of the $U(1)_A$ axial symmetry is independent of the specific parameter tuning within the studied range.

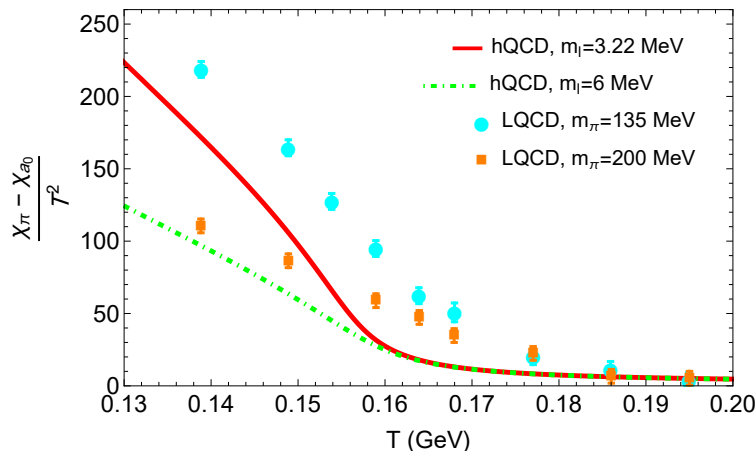


FIG. 9: The color online is similar to Fig. 8 with case II parameterization.

C. Topological susceptibility

Using the WTI associated with chiral symmetry, it can be demonstrated that the topological susceptibility is linked to the chiral- and $U(1)_A$ partner structures in the meson susceptibility functions. Therefore, the topological susceptibility can also be considered as an indicator of the strength of $U(1)_A$ symmetry breaking during the chiral phase transition. We numerically evaluate χ_{top} in Eq.(78), with the holographic QCD estimates on the χ_π and χ_{η_l} susceptibilities, as a function of temperature. In Fig. 10, we illustrate the temperature dependence of the topological susceptibility $\chi_{\text{top}}^{1/4}$, where we have taken the absolute value of χ_{top} , and compare it with LQCD data, NJL model, and linear sigma model (LSM). For case I (left panel), the value of $\chi_{\text{top}}^{1/4}(T = 0)$ at the light quark mass $m_l = 7.5$ MeV, which corresponds to the physical pion mass, is larger than the values obtained using other methods, possibly due to the fact that the physical quark mass used in other models is $m_l \sim 5$ MeV. Therefore, we also consider the case $m_l = 5$ MeV and the $\chi_{\text{top}}^{1/4}(T = 0)$ is in agreement with other models. However, in both cases of two light quark masses, the temperature behaviour is the same, and the $\chi_{\text{top}}^{1/4}$ declines more rapidly than others near the pseudocritical temperature. As we demonstrated in the previous subsection, in our model, the qualitative behavior of the indicator of $U(1)_A$ axial anomaly as a function of temperature is not consistent with LQCD, and it decreases sharply near the pseudocritical temperature. This feature causes the $\chi_{\text{top}}^{1/4}$ to decrease more sharply than in other models around the pseudocritical temperature. However, at higher temperatures our results show more persistent compare to other approaches. This slower suppression in our model points to specific features of the holographic gravitational dual. The dynamics of the axial anomaly and topological sectors are encoded in the structure of the bulk fields and their interactions. This could stem from the large- N_c nature underlying holographic constructions, where certain topological effects are enhanced, or from the specific choice of the gravitational background that does not fully capture the deconfining dynamics of the gauge theory. Overall, we can conclude that the qualitative behaviour of our model is similar to other approaches, as the value of $\chi_{\text{top}}^{1/4}$ is almost constant for $T < T_{pc}$. Then, around the $T \sim T_{pc}$, the curve decreases sharply, and finally, it slowly decreases for $T > T_{pc}$. The qualitative behaviour of $\chi_{\text{top}}^{1/4}$ for case II (right panel of Fig. 10) is not better than case I in comparison with other approaches.

The effect of $U(1)_A$ symmetry breaking was introduced through the determinant term in our model. The strength of the determinant term is controlled by the coupling parameter γ . To analyze the effect of the determinant term, we computed the topological susceptibility for different values of γ . As shown in Fig. 11, for a fixed light quark mass ($m_l = 7.5$ MeV or 5 MeV), a larger negative value of γ simply shifts the entire $\chi_{\text{top}}^{1/4}$ curve to a higher overall magnitude. Conversely, a smaller magnitude yields a lower curve. Crucially, the functional shape of the curve remains unchanged. This result has a significant physical implication. It demonstrates that in our model, the determinant term acts primarily as a static background source for topological effects, scaling their overall intensity up or down. However, it fails to modify the underlying dynamical response of the topological sectors. The gravitational background, which dictates how the system evolves, still forces the topological susceptibility to be strongly tied to the chiral transition scale, regardless of the value of γ .

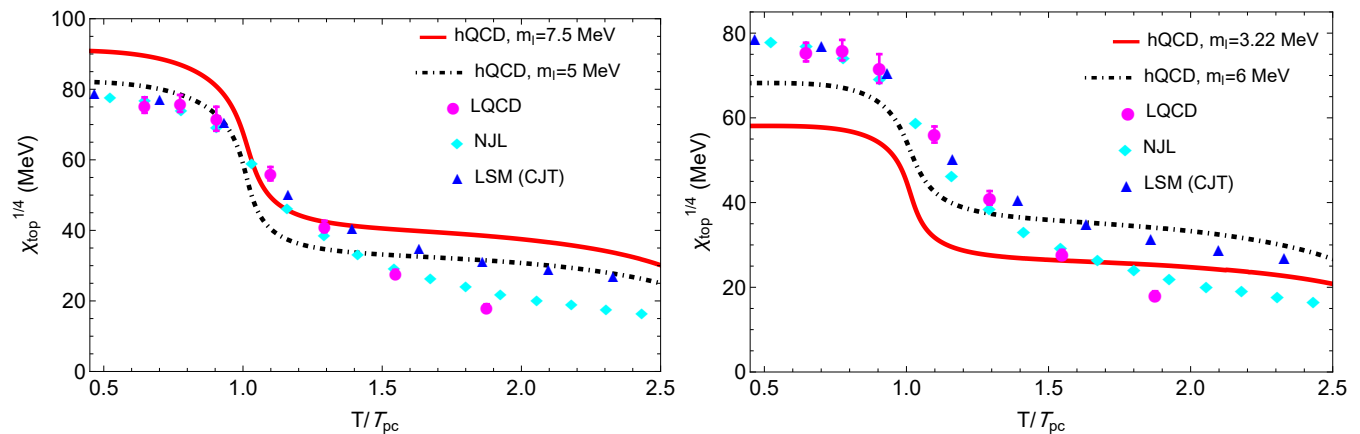


FIG. 10: The topological susceptibilities as a function of temperature at different light quark masses for case I (left) and II (right). The other approaches are LQCD [17], NJL [12], and LSM (CJT) [15].

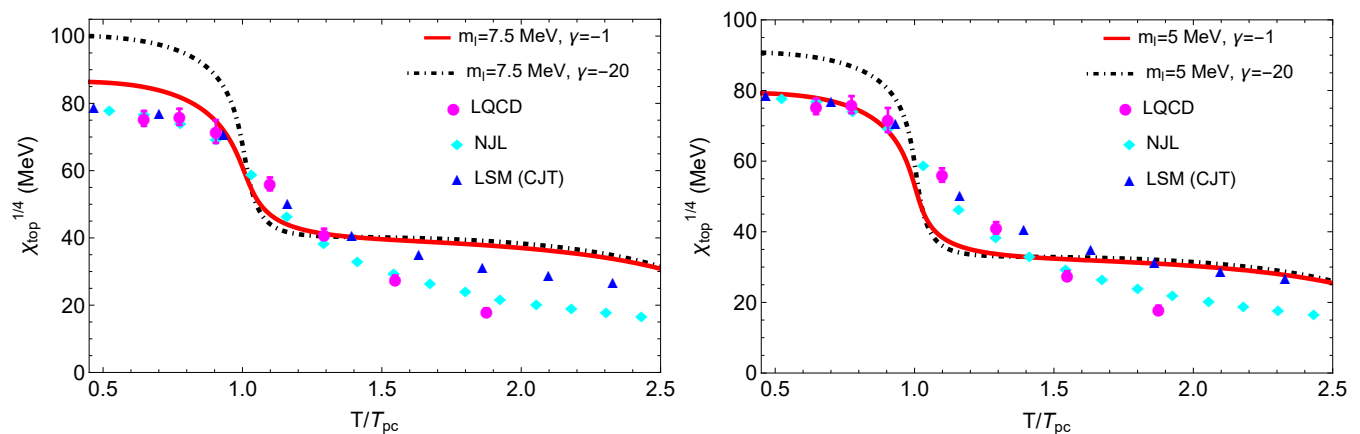


FIG. 11: Left panel: The topological susceptibilities as a function of temperature at light quark masses $m_l = 7.5$ MeV for different values of the determinant term's coupling as $\gamma = -1$ (solid red line) and $\gamma = -20$ (dot-dashed black line). Right panel: The color online is similar to the right panel for the light quark masses $m_l = 5$ MeV.

VI. CONCLUSIONS

In this work, we analyzed the finite-temperature restoration of chiral and $U(1)_A$ symmetries within the framework of a soft-wall holographic QCD model. Two specific parameterizations, denoted as Case I and Case II, were employed, both tuned to yield a physical pion mass and a chiral pseudocritical temperature of approximately 155 MeV. The primary observables were the quark condensates, meson screening masses, meson susceptibilities, and the topological susceptibility.

Our calculations demonstrate that the model robustly predicts a smooth chiral crossover transition. The temperature evolution of the light-quark condensate σ_l shows a smooth decrease, with its inflection point defining a pseudocritical temperature of $T_{pc} = 0.157$ GeV for Case I and $T_{pc} = 0.154$ GeV for Case II. This crossover behavior is a key feature of QCD with physical quark masses. The behavior of meson screening masses further confirms the restoration of chiral symmetry. The computed masses for the chiral partners (π , σ) and (η , a_0) become degenerate around T_{pc} , a direct signal of the effective restoration of chiral symmetry. This finding is quantitatively consistent with results from lattice QCD and effective models, such as the NJL model.

The analysis of meson susceptibilities provides a complementary and rigorous test. The differences $\chi_\pi - \chi_\sigma$ and $\chi_\eta - \chi_{a_0}$, which serve as indicators for chiral symmetry restoration, approach zero sharply around T_{pc} for both model parameterizations. The associated pseudocritical temperatures extracted from these indicators align with those obtained from the quark condensate, supporting a consistent picture of chiral restoration.

A central finding of this study concerns the fate of the $U(1)_A$ symmetry. The indicator $\chi_\pi - \chi_{a_0}$, which measures explicit $U(1)_A$ breaking due to the anomaly, vanishes near $T \sim 0.190$ GeV. This result, which holds for both Case I and Case II, indicates that within our holographic setup, the restoration scales for chiral and $U(1)_A$ symmetries do not coincide, which suggests a possible separation between these scales. Despite the inconsistency of the indicator

of $U(1)_A$ axial anomaly as a function of temperature with LQCD for temperatures $T < 0.175$ GeV, the restoration point match together.

The gravitational dual and the incorporated determinant term, parameterized by γ , tie the dynamics of the axial anomaly to the chiral order parameter. While varying γ alters the overall magnitude of anomaly-related quantities like the topological susceptibility, it does not decouple their temperature evolution from the chiral transition. This suggests that a more intricate holographic mechanism, perhaps involving independent bulk dynamics for topological sectors, is required to capture the potential persistence of $U(1)_A$ breaking effects above T_{pc} .

The topological susceptibility $\chi_{top}^{1/4}$, calculated via the Ward-Takahashi identity, exhibits a characteristic temperature dependence: it remains nearly constant for $T < T_{pc}$, drops sharply around the transition, and then slowly decreases at higher temperatures. While this qualitative trend agrees with other approaches, the detailed comparison reveals that our model predicts a more pronounced drop near T_{pc} and a slower subsequent suppression. This behavior is a direct consequence of the effect of the chiral symmetry restoration on the $U(1)_A$ axial anomaly in our framework.

In summary, the soft-wall holographic model successfully describes key aspects of the chiral phase transition, including the crossover nature, the degeneracy of chiral partners, and the associated susceptibility patterns. Moreover, it provides a separate restoration scale for chiral and $U(1)_A$ symmetries. Future improvements of the model should aim to introduce more independent elements into the gravitational dual, allowing for a better description of the $U(1)_A$ anomaly for achieving a closer alignment with the emerging picture from first-principles lattice QCD studies.

ACKNOWLEDGMENTS

This work is supported in part by the National Natural Science Foundation of China (NSFC) Grant Nos: 12235016, 12221005, 12275108, and W2433019.

Appendix A: The value of mass parameters

$$M_s^{a,b}(z) = \begin{pmatrix} (\frac{3}{2}\chi_l^2)_{I_{3 \times 3}} & 0 & 0 & 0 \\ 0 & (\frac{1}{2}(\chi_l^2 + \chi_l\chi_s + \chi_s^2))_{I_{4 \times 4}} & 0 & 0 \\ 0 & 0 & \frac{1}{2}(\chi_l^2 + 2\chi_s^2) & \frac{1}{\sqrt{2}}(\chi_l^2 - \chi_s^2) \\ 0 & 0 & \frac{1}{\sqrt{2}}(\chi_l^2 - \chi_s^2) & \frac{1}{2}(2\chi_l^2 + \chi_s^2) \end{pmatrix}, \quad (A1)$$

$$M_{det}^{a,b}(z) = \begin{pmatrix} (\frac{-1}{8}\chi_s)_{I_{3 \times 3}} & 0 & 0 & 0 \\ 0 & (\frac{-1}{8}\chi_l)_{I_{4 \times 4}} & 0 & 0 \\ 0 & 0 & \frac{-1}{24}(4\chi_l - \chi_s) & \frac{-1}{12\sqrt{2}}(\chi_l - \chi_s) \\ 0 & 0 & \frac{-1}{12\sqrt{2}}(\chi_l - \chi_s) & \frac{1}{12}(2\chi_l + \chi_s) \end{pmatrix}, \quad (A2)$$

$$M_A^{a,b}(z) = \begin{pmatrix} (\chi_l^2)_{I_{3 \times 3}} & 0 & 0 & 0 \\ 0 & (\frac{1}{4}(\chi_l + \chi_s)^2)_{I_{4 \times 4}} & 0 & 0 \\ 0 & 0 & \frac{1}{3}(\chi_l^2 + 2\chi_s^2) & \frac{\sqrt{2}}{3}(\chi_l^2 - \chi_s^2) \\ 0 & 0 & \frac{\sqrt{2}}{3}(\chi_l^2 - \chi_s^2) & \frac{1}{3}(2\chi_l^2 + \chi_s^2) \end{pmatrix}, \quad (A3)$$

where the index $a, b = 9$ corresponds to the singlet state.

-
- [1] T. Hatsuda and T. Kunihiro, QCD phenomenology based on a chiral effective Lagrangian, *Phys. Rept.* **247**, 221 (1994), [arXiv:hep-ph/9401310](https://arxiv.org/abs/hep-ph/9401310).
[2] S. Weinberg, The U(1) Problem, *Phys. Rev. D* **11**, 3583 (1975).
[3] T. D. Cohen, The High temperature phase of QCD and U(1)-A symmetry, *Phys. Rev. D* **54**, R1867 (1996), [arXiv:hep-ph/9601216](https://arxiv.org/abs/hep-ph/9601216).

- [4] S. Aoki, H. Fukaya, and Y. Taniguchi, Chiral symmetry restoration, eigenvalue density of Dirac operator and axial $U(1)$ anomaly at finite temperature, *Phys. Rev. D* **86**, 114512 (2012), [arXiv:1209.2061 \[hep-lat\]](#).
- [5] A. Bazavov et al. (HotQCD), The chiral transition and $U(1)_A$ symmetry restoration from lattice QCD using Domain Wall Fermions, *Phys. Rev. D* **86**, 094503 (2012), [arXiv:1205.3535 \[hep-lat\]](#).
- [6] T. Bhattacharya et al., QCD Phase Transition with Chiral Quarks and Physical Quark Masses, *Phys. Rev. Lett.* **113**, 082001 (2014), [arXiv:1402.5175 \[hep-lat\]](#).
- [7] S. Aoki, Y. Aoki, H. Fukaya, S. Hashimoto, C. Rohrhofer, and K. Suzuki (JLQCD), Role of the axial $U(1)$ anomaly in the chiral susceptibility of QCD at high temperature, *PTEP* **2022**, 023B05 (2022), [arXiv:2103.05954 \[hep-lat\]](#).
- [8] A. Bazavov et al., Meson screening masses in (2+1)-flavor QCD, *Phys. Rev. D* **100**, 094510 (2019), [arXiv:1908.09552 \[hep-lat\]](#).
- [9] H.-T. Ding, J.-B. Gu, S.-T. Li, and R. Thakkar, Chiral condensates and screening masses of neutral pseudoscalar mesons from lattice QCD at physical quark masses, *Phys. Rev. D* **111**, 074513 (2025), [arXiv:2501.11262 \[hep-lat\]](#).
- [10] A. Gómez Nicola and J. Ruiz de Elvira, Pseudoscalar susceptibilities and quark condensates: chiral restoration and lattice screening masses, *JHEP* **03**, 186, [arXiv:1602.01476 \[hep-ph\]](#).
- [11] A. Gomez Nicola and J. Ruiz de Elvira, Patterns and partners for chiral symmetry restoration, *Phys. Rev. D* **97**, 074016 (2018), [arXiv:1704.05036 \[hep-ph\]](#).
- [12] C.-X. Cui, J.-Y. Li, S. Matsuzaki, M. Kawaguchi, and A. Tomiya, New interpretation of the chiral phase transition: Violation of the trilemma in QCD, *Phys. Rev. D* **105**, 114031 (2022), [arXiv:2106.05674 \[hep-ph\]](#).
- [13] C.-X. Cui, J.-Y. Li, S. Matsuzaki, M. Kawaguchi, and A. Tomiya, New Aspect of Chiral $SU(2)$ and $U(1)$ Axial Breaking in QCD, *Particles* **7**, 237 (2024), [arXiv:2205.12479 \[hep-ph\]](#).
- [14] M. Kawaguchi, S. Matsuzaki, and A. Tomiya, Nonperturbative flavor breaking in topological susceptibility at chiral crossover, *Phys. Lett. B* **813**, 136044 (2021), [arXiv:2003.11375 \[hep-ph\]](#).
- [15] M. Kawaguchi, S. Matsuzaki, and A. Tomiya, Analysis of nonperturbative flavor violation at chiral crossover criticality in QCD, *Phys. Rev. D* **103**, 054034 (2021), [arXiv:2005.07003 \[hep-ph\]](#).
- [16] M. Kawaguchi and D. Suenaga, Fate of the topological susceptibility in two-color dense QCD, *JHEP* **08**, 189, [arXiv:2305.18682 \[hep-ph\]](#).
- [17] S. Borsanyi et al., Calculation of the axion mass based on high-temperature lattice quantum chromodynamics, *Nature* **539**, 69 (2016), [arXiv:1606.07494 \[hep-lat\]](#).
- [18] C. Bonati, M. D'Elia, M. Mariti, G. Martinelli, M. Mesiti, F. Negro, F. Sanfilippo, and G. Villadoro, Axion phenomenology and θ -dependence from $N_f = 2 + 1$ lattice QCD, *JHEP* **03**, 155, [arXiv:1512.06746 \[hep-lat\]](#).
- [19] P. Petreczky, H.-P. Schadler, and S. Sharma, The topological susceptibility in finite temperature QCD and axion cosmology, *Phys. Lett. B* **762**, 498 (2016), [arXiv:1606.03145 \[hep-lat\]](#).
- [20] A. Tomiya, G. Cossu, S. Aoki, H. Fukaya, S. Hashimoto, T. Kaneko, and J. Noaki, Evidence of effective axial $U(1)$ symmetry restoration at high temperature QCD, *Phys. Rev. D* **96**, 034509 (2017), [Addendum: *Phys.Rev.D* 96, 079902 (2017)], [arXiv:1612.01908 \[hep-lat\]](#).
- [21] S. Aoki, Y. Aoki, G. Cossu, H. Fukaya, S. Hashimoto, T. Kaneko, C. Rohrhofer, and K. Suzuki (JLQCD), Study of the axial $U(1)$ anomaly at high temperature with lattice chiral fermions, *Phys. Rev. D* **103**, 074506 (2021), [arXiv:2011.01499 \[hep-lat\]](#).
- [22] M. I. Buchoff et al., QCD chiral transition, $U(1)_A$ symmetry and the dirac spectrum using domain wall fermions, *Phys. Rev. D* **89**, 054514 (2014), [arXiv:1309.4149 \[hep-lat\]](#).
- [23] H.-T. Ding, S.-T. Li, X.-D. Wang, Y. Zhang, A. Tomiya, and S. Mukherjee, Correlated Dirac Eigenvalues and Axial Anomaly in Chiral Symmetric QCD, *PoS LATTICE2021*, 619 (2022), [arXiv:2112.00465 \[hep-lat\]](#).
- [24] J. M. Maldacena, The Large N limit of superconformal field theories and supergravity, *Adv. Theor. Math. Phys.* **2**, 231 (1998), [arXiv:hep-th/9711200](#).
- [25] E. Witten, Anti-de Sitter space and holography, *Adv. Theor. Math. Phys.* **2**, 253 (1998), [arXiv:hep-th/9802150](#).
- [26] A. Karch and E. Katz, Adding flavor to AdS / CFT, *JHEP* **06**, 043, [arXiv:hep-th/0205236](#).
- [27] T. Sakai and S. Sugimoto, Low energy hadron physics in holographic QCD, *Prog. Theor. Phys.* **113**, 843 (2005), [arXiv:hep-th/0412141](#).
- [28] J. Erlich, E. Katz, D. T. Son, and M. A. Stephanov, QCD and a holographic model of hadrons, *Phys. Rev. Lett.* **95**, 261602 (2005), [arXiv:hep-ph/0501128](#).
- [29] L. Da Rold and A. Pomarol, Chiral symmetry breaking from five dimensional spaces, *Nucl. Phys. B* **721**, 79 (2005), [arXiv:hep-ph/0501218](#).
- [30] A. Karch, E. Katz, D. T. Son, and M. A. Stephanov, Linear confinement and AdS/QCD, *Phys. Rev. D* **74**, 015005 (2006), [arXiv:hep-ph/0602229](#).
- [31] S. S. Gubser and A. Nellore, Mimicking the QCD equation of state with a dual black hole, *Phys. Rev. D* **78**, 086007 (2008), [arXiv:0804.0434 \[hep-th\]](#).
- [32] S. S. Gubser, A. Nellore, S. S. Pufu, and F. D. Rocha, Thermodynamics and bulk viscosity of approximate black hole duals to finite temperature quantum chromodynamics, *Phys. Rev. Lett.* **101**, 131601 (2008), [arXiv:0804.1950 \[hep-th\]](#).
- [33] U. Gursoy and E. Kiritsis, Exploring improved holographic theories for QCD: Part I, *JHEP* **02**, 032, [arXiv:0707.1324 \[hep-th\]](#).
- [34] U. Gursoy, E. Kiritsis, and F. Nitti, Exploring improved holographic theories for QCD: Part II, *JHEP* **02**, 019, [arXiv:0707.1349 \[hep-th\]](#).
- [35] P. Colangelo, F. Giannuzzi, S. Nicotri, and V. Tangorra, Temperature and quark density effects on the chiral condensate: An AdS/QCD study, *Eur. Phys. J. C* **72**, 2096 (2012), [arXiv:1112.4402 \[hep-ph\]](#).

- [36] L.-X. Cui and Y.-L. Wu, Thermal Mass Spectra of Scalar and Pseudo-Scalar Mesons in IR-improved Soft-Wall AdS/QCD Model with Finite Chemical Potential, *Mod. Phys. Lett. A* **28**, 1350132 (2013), [arXiv:1302.4828 \[hep-ph\]](#).
- [37] S. P. Bartz and T. Jacobson, Chiral Phase Transition and Meson Melting from AdS/QCD, *Phys. Rev. D* **94**, 075022 (2016), [arXiv:1607.05751 \[hep-ph\]](#).
- [38] K. Chelabi, Z. Fang, M. Huang, D. Li, and Y.-L. Wu, Realization of chiral symmetry breaking and restoration in holographic QCD, *Phys. Rev. D* **93**, 101901 (2016), [arXiv:1511.02721 \[hep-ph\]](#).
- [39] K. Chelabi, Z. Fang, M. Huang, D. Li, and Y.-L. Wu, Chiral Phase Transition in the Soft-Wall Model of AdS/QCD, *JHEP* **04**, 036, [arXiv:1512.06493 \[hep-ph\]](#).
- [40] Z. Fang, S. He, and D. Li, Chiral and Deconfining Phase Transitions from Holographic QCD Study, *Nucl. Phys. B* **907**, 187 (2016), [arXiv:1512.04062 \[hep-ph\]](#).
- [41] Z. Fang, Y.-L. Wu, and L. Zhang, Chiral phase transition and meson spectrum in improved soft-wall AdS/QCD, *Phys. Lett. B* **762**, 86 (2016), [arXiv:1604.02571 \[hep-ph\]](#).
- [42] D. Li and M. Huang, Chiral phase transition of QCD with $N_f = 2 + 1$ flavors from holography, *JHEP* **02**, 042, [arXiv:1610.09814 \[hep-ph\]](#).
- [43] S. P. Bartz and T. Jacobson, Chiral phase transition at finite chemical potential in 2+1 -flavor soft-wall anti-de Sitter space QCD, *Phys. Rev. C* **97**, 044908 (2018), [arXiv:1801.00358 \[hep-ph\]](#).
- [44] H. A. Ahmed, M. Kawaguchi, and M. Huang, Effect of charm quark on chiral phase transition in $N_f=2+1+1$ holographic QCD, *Phys. Rev. D* **110**, 046002 (2024), [arXiv:2401.04355 \[hep-ph\]](#).
- [45] X. Cao, S. Qiu, H. Liu, and D. Li, Thermal properties of light mesons from holography, *JHEP* **08**, 005, [arXiv:2102.10946 \[hep-ph\]](#).
- [46] X. Cao, M. Baggioli, H. Liu, and D. Li, Pion dynamics in a soft-wall AdS-QCD model, *JHEP* **12**, 113, [arXiv:2210.09088 \[hep-ph\]](#).
- [47] T. Gherghetta, J. I. Kapusta, and T. M. Kelley, Chiral symmetry breaking in the soft-wall AdS/QCD model, *Phys. Rev. D* **79**, 076003 (2009), [arXiv:0902.1998 \[hep-ph\]](#).
- [48] M. Rinaldi, F. A. Ceccopieri, and V. Vento, The pion in the graviton soft-wall model: phenomenological applications, *Eur. Phys. J. C* **82**, 626 (2022), [arXiv:2204.09974 \[hep-ph\]](#).
- [49] A. Ballon-Bayona, T. Frederico, L. A. H. Mamani, and W. de Paula, Dynamical holographic QCD model for spontaneous chiral symmetry breaking and confinement, *Phys. Rev. D* **108**, 106016 (2023), [arXiv:2308.07503 \[hep-ph\]](#).
- [50] A. Cherman, T. D. Cohen, and E. S. Werbos, The Chiral condensate in holographic models of QCD, *Phys. Rev. C* **79**, 045203 (2009), [arXiv:0804.1096 \[hep-ph\]](#).
- [51] Z. Fang, Y.-L. Wu, and L. Zhang, Octet meson spectra and chiral phase diagram in the improved soft-wall AdS/QCD model, *Phys. Rev. D* **100**, 054008 (2019), [arXiv:1904.04695 \[hep-ph\]](#).
- [52] X. Cao, H. Liu, and D. Li, Pion quasiparticles and QCD phase transitions at finite temperature and isospin density from holography, *Phys. Rev. D* **102**, 126014 (2020), [arXiv:2009.00289 \[hep-ph\]](#).
- [53] M. Cheng et al., Meson screening masses from lattice QCD with two light and the strange quark, *Eur. Phys. J. C* **71**, 1564 (2011), [arXiv:1010.1216 \[hep-lat\]](#).
- [54] Y. Jiang, K. Ren, T. Xia, and P. Zhuang, Meson Screening Mass in a Strongly Coupled Pion Superfluid, *Eur. Phys. J. C* **71**, 1822 (2011), [arXiv:1104.0094 \[hep-ph\]](#).